

# Rate of formation and dissolution of mercury sulfide nanoparticles: The dual role of natural organic matter

Aaron J. Slowey\*

Water Resources Discipline, United States Geological Survey, 345 Middlefield Road, Mail Stop 466, Menlo Park, CA, USA

Received 11 December 2009; accepted in revised form 6 May 2010; available online 13 May 2010

## Abstract

Mercury is a global contaminant of concern due to its transformation by microorganisms to form methylmercury, a toxic species that accumulates in biological tissues. The effect of dissolved organic matter (DOM) isolated from natural waters on reactions between mercury(II) (Hg) and sulfide (S(-II)) to form  $\text{HgS}_{(s)}$  nanoparticles across a range of Hg and S(-II) concentrations was investigated. Hg was equilibrated with DOM, after which S(-II) was added. Dissolved Hg ( $\text{Hg}_{\text{aq}}$ ) was periodically quantified using ultracentrifugation and chemical analysis following the addition of S(-II). Particle size and identity were determined using dynamic light scattering and X-ray absorption spectroscopy. S(-II) reacts with Hg to form 20 to 200 nm aggregates consisting of 1–2 nm  $\text{HgS}_{(s)}$  subunits that are more structurally disordered than metacinnabar in the presence of  $2 \times 10^{-9}$  to  $8 \times 10^{-6}$  M Hg and  $10 \text{ (mg C) L}^{-1}$  DOM. Some of the  $\text{HgS}_{(s)}$  nanoparticle aggregates are subsequently dissolved by DOM and (re)precipitated by S(-II) over periods of hours to days. At least three fractions of Hg–DOM species were observed with respect to reactivity toward S(-II): 0.3  $\mu\text{mol}$  reactive Hg per mmol C (60 percent), 0.1  $\mu\text{mol}$  per mmol C (20 percent) that are kinetically hindered, and another 0.1  $\mu\text{mol}$  Hg per mmol C (20 percent) that are inert to reaction with S(-II). Following an initial S(-II)-driven precipitation of  $\text{HgS}_{(s)}$ ,  $\text{HgS}_{(s)}$  was dissolved by DOM or organic sulfur compounds.  $\text{HgS}_{(s)}$  formation during this second phase was counterintuitively favored by lower S(-II) concentrations, suggesting surface association of DOM moieties that are less capable of dissolving  $\text{HgS}_{(s)}$ . DOM partially inhibits  $\text{HgS}_{(s)}$  formation and mediates reactions between Hg and S(-II) such that  $\text{HgS}_{(s)}$  is susceptible to dissolution. These findings indicate that Hg accessibility to microorganisms could be controlled by kinetic (intermediate) species in the presence of S(-II) and DOM, undermining the premise that equilibrium Hg species distributions should correlate to the extent or rate of Hg methylation in soils and sediments.

Published by Elsevier Ltd.

## 1. INTRODUCTION

Organic matter performs several functions in the biogeochemical transport and transformation of mercury, including methylation by microorganisms in water, soils, and sediments (Ravichandran, 2004; Fitzgerald et al., 2007). Methylmercury can accumulate in low trophic-level organisms such as phytoplankton and zooplankton and magnify up the food chain. For example, Stewart et al. (2008) found that a reservoir containing at most 0.04 ng  $\text{L}^{-1}$  of filterable

methylmercury (MeHg) was inhabited by zooplankton containing 4–77 (ng MeHg) (g biomass) $^{-1}$  and bass containing 1500 (ng MeHg) (g biomass) $^{-1}$ . Magnification of methylmercury can expose humans to unhealthy amounts of methylmercury through fish consumption, possibly causing teratogenic effects, increased risk of heart attack, and endocrine disruption (Mergler et al., 2007). Methylmercury can also cause neurological, behavioral, and reproductive effects and death in wildlife (Scheuhammer et al., 2007; Eagles-Smith and Ackerman, 2009).

Predicting the reactivity of a small, yet ecologically worrisome, amount of inorganic mercury(II) (Hg) with respect to methylation has proven difficult. Certain Hg species are assumed to be more accessible to microorganisms, either by

\* Corresponding author. Tel.: +1 650 329 5474.  
E-mail address: [aslowey@usgs.gov](mailto:aslowey@usgs.gov)

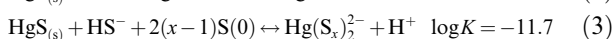
diffusive or active transport across cell membranes (Schaefer and Morel, 2009). The amount of bioaccessible Hg is believed to correlate to the extent or rate of Hg methylation (Merritt and Amirbahman, 2009). Mercury methylation has been found to occur under anaerobic, and therefore, typically organic rich, conditions in which some species of sulfate and Fe(III)-reducing bacteria (SRB and FeRB) are active (King et al., 2001; Fleming et al., 2006; Han et al., 2008b; Windham-Myers et al., 2009). Organic matter in soils and sediments includes dissolved organic molecules that are exuded by plant roots and microorganisms, derived from the biological degradation of plant tissues (Hedges and Oades, 1997), and that accumulate in anaerobic porewater (Kalbitz et al., 2000) typically in excess of Hg by a factor of  $10^6$  (Hall et al., 2008; Marvin-DiPasquale et al., 2009). Thus, S(-II), dissolved organic matter (DOM), and Fe(II) are some of the constituents that may affect the accessibility of Hg to microorganisms and therefore, the extent to which microorganisms methylate Hg.

Aquatic DOM complexes Hg (Haitzer et al., 2002), mediates reactions between Hg and S(-II) (Ravichandran et al., 1999; Deonaraine and Hsu-Kim, 2009), and dissolves  $\text{HgS}_{(s)}$  (Ravichandran et al., 1998; Waples et al., 2005). Aquatic DOM consists of thousands of analogous, but not identical, less than 1000 Da hydrophilic molecules (Aiken and Malcolm, 1987; Chin et al., 1994; Lead et al., 2000a; Reemtsma et al., 2008).  $\text{Hg}^{2+}$ , a soft, or B-type, metal cation, reacts readily with soft bases, of which inorganic sulfide (S(-II)) and organic thiolate ( $\text{RS}^-$ ) are most favorable (Haitzer et al., 2002). Weaker associations between  $\text{Hg}^{2+}$  and harder bases such as nitrogen- and oxygen-bearing organic functional groups ( $\text{RCN}^-$ ,  $\text{RCOO}^-$ ) can also form (Skylberg, 2008). Hg–DOM complex stability—as an average of an ensemble of chemically heterogeneous species ( $K^* = [\text{HgDOM}]/[\text{Hg}^{2+}][\text{DOM}]$ )—decreases as Hg saturates strongly binding ligands (e.g.,  $\text{Hg}(\text{RS})_2$ ) and progressively saturates weaker ligands at higher Hg/DOM ratios (Haitzer et al., 2002). Hg–DOM stability is also affected by pH and the duration  $\text{Hg}^{2+}$  coexists with DOM (Haitzer et al., 2003; Gasper et al., 2007).

The occurrence of  $\text{HgS}_{(s)}$  has been documented for mines and industrial sites (Barnett et al., 1997; Kim et al., 2000, 2004; Slowey et al., 2005a,b; Liu et al., 2006) but is uncertain in more diffusely contaminated systems such as the Florida Everglades and the Arctic (Gilmour et al., 1998; Oiffer and Siciliano, 2009). The occurrence of  $\text{HgS}_{(s)}$  in soils and sediments on the basis of Hg species distribution models depends on what  $\text{HgS}_{(s)}$  formation/dissolution reactions are considered. The reaction



has been frequently included in Hg species distribution models with an estimated  $\log K = -10$ , implying that  $\text{HgS}_{(s)}$  is  $10^{1.7}$  to  $10^{26.4}$  times more soluble than if it underwent other proposed dissolution reactions:



(Paquette and Helz, 1997; Jay et al., 2000), assuming for simplicity that the activities of  $\text{H}^+$  and  $\text{HS}^-$  are equal. As

explained by Skylberg (2008), experimental evidence undermines the plausibility of  $\text{HOHgSH}$  (or  $\text{HgS}\cdot\text{H}_2\text{O}$  or  $\text{HgS}^0$ ) (Daskalakis and Helz, 1993). Even if  $\text{HgS}^0$  did exist, the  $\log K$  value of reaction (1) could range from  $-22.3$  to  $-10.0$  (Skylberg, 2008). Inclusion of reaction (1) in a model and choice of an implausibly high  $\log K$  could erroneously suggest that  $\text{HgS}_{(s)}$  is absent.  $\text{HgS}_{(s)}$  formation is sometimes suppressed in a model, based on the assumption that Hg forms inert Hg–thiol complexes with DOM and soil humus prior to being exposed to S(-II) (Skylberg, 2008). However, little data are available to evaluate whether DOM or soil humus inhibits the formation of  $\text{HgS}_{(s)}$  in soils.

Depending on Hg concentration, dissolved thiol and hydrophobic organic ligands can inhibit the formation and particle growth of  $\text{HgS}_{(s)}$  (Ravichandran et al., 1999). While this research was the first to quantify the extent to which DOM affects Hg reactivity toward S(-II), phase separation was approximate and particle size was not measured, such that the formation and temporal stability of  $\text{HgS}_{(s)}$  nanoparticles less than approximately 20 nm was not determined. Without time-resolved data, the physicochemical stability of  $\text{HgS}_{(s)}$  remained poorly understood following the work of Ravichandran et al. (1999). Using similar laboratory systems, Deonaraine and Hsu-Kim (2009) show that increasing concentrations of DOM can progressively slow the growth, but not inhibit the formation, of  $\text{HgS}_{(s)}$ . Unresolved questions from these studies include the degree to which Hg and S(-II) control the rate and extent of  $\text{HgS}_{(s)}$  formation in the presence of DOM. In addition, neither study obtained time-resolved quantitative chemical data to monitor  $\text{HgS}_{(s)}$  dissolution subsequent to or coincident with  $\text{HgS}_{(s)}$  formation, which other studies suggest may also affect Hg reactivity in soils and sediments.

While  $\text{HgS}_{(s)}$  is likely more prevalent in aquatic ecosystems than previously thought based on updated formation/dissociation constants, it would also be more soluble than predicted by models that neglect  $\text{HgS}_{(s)}$  dissolution by DOM. While DOM can dissolve micrometer-sized cinnabar ( $\alpha\text{-HgS}$ ) (Ravichandran et al., 1998; Waples et al., 2005), the most stable form of  $\text{HgS}_{(s)}$ , the solubility of  $\text{HgS}_{(s)}$  that originally forms in the presence of DOM remains elusive and yet is more relevant to most soils and sediments. Electron diffraction and chemical extraction studies indicate that metacinnabar ( $\beta\text{-HgS}$ ) nanoparticles in contaminated soils are poorly crystalline and more soluble in strong acid than synthetic  $\text{HgS}_{(s)}$  minerals (Barnett et al., 1997; Han et al., 2008a).

To summarize, the importance of  $\text{HgS}_{(s)}$  to Hg methylation in most natural systems remains unclear due to inconclusive thermodynamic interpretations of field data and limited understanding of the effect of DOM on the reaction between  $\text{Hg}_{\text{aq}}$  and S(-II) and the stability of  $\text{HgS}_{(s)}$ . This study extends previous research (Ravichandran et al., 1999; Deonaraine and Hsu-Kim, 2009) by quantifying dissolved Hg ( $\text{Hg}_{\text{aq}}$ ) with lower particle size exclusion ( $>5$  nm), *in situ* S(-II) quantification, and parallel particle sizing and identification using dynamic light scattering and X-ray absorption spectroscopy. Experiments included low S(-II)/Hg to investigate  $\text{HgS}_{(s)}$  formation and stability under conditions that are apparently conducive to Hg

methylation (Hammerschmidt et al., 2008; Mitchell and Gilmour, 2008; Hollweg et al., 2009; Marvin-DiPasquale et al., 2009). I also build on the work of Ravichandran et al. (1998) and Waples et al. (2005) by quantifying  $\text{Hg}_{\text{aq}}$  during and immediately after  $\text{HgS}_{(\text{s})}$  formed in the presence of DOM in systems containing lower Hg/DOM ratios.  $\text{Hg}_{\text{aq}}$  was also monitored over nearly two weeks to determine whether Hg–DOM–S(-II) systems reach equilibrium. The results clarify the importance of DOM, not just as a group of Hg-binding ligands, but also as a mediator of  $\text{Hg}_{\text{aq}}$ –S(-II) reactions and  $\text{HgS}_{(\text{s})}$  nanoparticle dissolution.

## 2. METHODS

### 2.1. Materials

Water used in experiments was deionized (18 M $\Omega$  cm), UV-irradiated, and pumped through a 10,000 Da filter (Barnstead Nanopure). Water was deoxygenated by boiling, purging with ultrahigh-purity (UHP)  $\text{N}_2$  and storage in a 98 percent  $\text{N}_2$ , 2 percent  $\text{H}_2$  Coy glove box (chamber gases were industrial grade and deoxygenated using a Pd catalyst). For lab-ware cleaning and digestion of samples for mercury analysis, bromine monochloride (BrCl) reagent was prepared by dissolving KBr and  $\text{KBrO}_3$  to 10 mM each in trace metal-grade 12 N HCl. All glassware was sonicated in detergent and then soaked sequentially in one percent by volume (v/v) KOH and 5 percent v/v aqua regia (1:3 volume-ratio of concentrated  $\text{HNO}_3$ :HCl) and rinsed with deionized water. Before reuse, polycarbonate ultracentrifuge tubes were separated according to prior mercury content and soaked in 2 percent v/v BrCl at room temperature for at least 18 h and sequentially rinsed with 0.1 N  $\text{HNO}_3$  and deionized water. Ten millimolar sulfide stock solutions were made by dissolving anhydrous sodium sulfide ( $\text{Na}_2\text{S}$ ), buffered with 10 mM boric acid ( $\text{H}_3\text{BO}_3$ ) (pH 8.3), and iodometrically standardized with a NIST potassium dichromate-standardized, alkaline-stabilized thiosulfate solution.  $\text{Na}_2\text{S}$  stock solutions were buffered to avoid severe alkaline perturbation of experimental systems. Boric acid was used to buffer  $\text{Na}_2\text{S}$  because other acids volatilized  $\text{H}_2\text{S}_{(\text{g})}$  when added to  $\text{Na}_2\text{S}$  stock solutions.

Suwannee River fulvic acid (SRFA), Suwannee River humic acid (SRHA), and Pony Lake fulvic acid (PLFA) (Malcolm et al., 1994; Brown et al., 2004) were obtained from the International Humic Substances Society, weighed using a microbalance, and dissolved in glass bottles with deoxygenated water to  $10.0 \pm 0.1$  (mg C)  $\text{L}^{-1}$  ( $0.833 \pm 0.009$  (mmol C)  $\text{L}^{-1}$ ), an intermediate concentration compared to typical surface waters and organic-rich soil pore waters (Thurman, 1985). The mass of isolate was computed based on its carbon content:  $0.5234$  (g C) (g SRFA) $^{-1}$ ,  $0.5263$  (g C) (g SRHA) $^{-1}$ ,  $0.5247$  (g C) (g PLFA) $^{-1}$ ; e.g.,  $10$  (mg C)  $\text{L}^{-1}$  is equivalent to  $19.1$  (mg SRFA)  $\text{L}^{-1}$ . The Hg content of dissolved SRFA, SRHA, and PLFA solutions was measured in  $10$  (mg C)  $\text{L}^{-1}$  DOM solutions amended with 1 percent v/v BrCl and found to be 0.18, 0.34, and 0.04 nM, respectively. On the basis of these measurements, the freeze-dried AOM isolates of SRFA, SRHA, and PLFA, contain 1.8, 3.6, and 0.42 ( $\mu\text{g Hg}$ ) (g dry AOM) $^{-1}$ . Dissolved

organic matter (DOM) solutions were refrigerated at 5 °C and used within two weeks.

### 2.2. Time-resolved mercury phase-distribution experiments

All experiments were conducted at  $22 \pm 2$  °C. DOM solutions were buffered to pH  $7.0 \pm 0.2$  with 10 mM sodium bicarbonate ( $\text{NaHCO}_3$ ) and perchloric acid ( $\text{HClO}_4$ ): 9.5 mM for SRFA, 6.9 mM for SRHA, and 7.0 mM for PLFA, determined on the basis of pH measurements of DOM containing a range of  $\text{HClO}_4$  concentrations over two weeks. DOM was amended with the specified amount of  $\text{HClO}_4$  and allowed to rest for one day to ensure consistency and amphoteric stability prior to adding Hg.  $\text{Hg}(\text{NO}_3)_2$  was added to DOM at five concentrations ranging over five orders of magnitude ( $0.001$ – $10$   $\mu\text{M}$ , giving mass ratios of  $0.01$ – $100$  ( $\mu\text{g Hg}$ ) (mg DOM) $^{-1}$ ) and allowed to react at room temperature for at least 11 h to form bonds between Hg and less abundant yet stronger organic ligands (Gasper et al., 2007). Prior to adding S(-II), samples were collected and later measured for Hg.  $\text{Hg}_{\text{aq}}$  recovered from these samples was less than what was added to the batch reactors, indicating that Hg adhered to the walls of the glass serum bottles (see Electronic annex (EA) for details).

After equilibrating the Hg–DOM solutions, S(-II) was added either as an instantaneous dose of aqueous sodium sulfide ( $\text{Na}_2\text{S}$ ) or by flowing  $\text{H}_2\text{S}_{(\text{g})}$  through the headspace of an enclosed vessel. For  $\text{Na}_2\text{S}$  amendments,  $\text{Na}_2\text{S}$ /boric acid ( $\text{H}_3\text{BO}_3$ ) (pH 8.3) was added to 40-mL Hg–DOM solutions in glass serum bottles to reach an initial concentration of  $140$   $\mu\text{M}$ , equivalent to 20 mole-percent of dissolved organic carbon. Each serum bottle was closed with a butyl rubber stopper and quiescently stored in an oxygen-free glove box. For  $\text{H}_2\text{S}_{(\text{g})}$  amendments,  $\text{Na}_2\text{S}$  was mixed with piperazine-*N,N'*-bis(2-ethanesulfonic acid) (PIPES) in a gas washing bottle (pH 7). S(-II) amendment commenced by bubbling  $5$   $\text{mL min}^{-1}$  UHP nitrogen through a diffuser in the gas washing bottle to carry  $\text{H}_2\text{S}_{(\text{g})}$  into the enclosed headspace of a 100 mL glass vessel initially containing 50 mL of stirred Hg–DOM solution.  $\text{CO}_2$  ( $1$   $\text{mL min}^{-1}$ ) was concurrently flowed through the headspace of the reactor to maintain pH  $7.1 \pm 0.2$  in all but one experiment. Buffering pH against S(-II)-related alkaline perturbation is required to not suddenly weaken Hg–DOM interactions that could induce rapid  $\text{HgS}_{(\text{s})}$  formation and aggregation.

Each batch reactor was swirled by hand prior to pipetting 1 mL samples into 1.5 mL,  $11 \times 34$  mm polycarbonate tubes, tilted at 30° from vertical in a rotor (TLA-120.2), and ultracentrifuged at 60,000 rpm (98,800–157,000 rcf ( $\times g$ ) across a 24.5–38.9 mm radius from the axis of rotation) for 30 min (Beckman Coulter Optima TLX ultracentrifuge) to separate  $>5$  nm particles from liquid while minimizing perturbations to DOM (e.g., molecular weight distribution) and avoiding filtration-induced aggregation (Buffle and Leppard, 1995). After ultracentrifugation, 0.8 mL of supernatant was withdrawn from the tube over about 20 s and transferred to a 1.5 mL plastic tube, amended with 3 percent v/v BrCl, tightly capped, stored at room temperature for 1 day, then refrigerated at 5 °C until analyzed for mercury. Control experiments indicate that ultracentrifugation

removed an insignificant amount of  $\text{Hg}_{\text{aq}}$  (see Annex for details). Ultracentrifugation, supernatant recovery, and Hg analysis introduced 2–5 percent error in  $\text{Hg}_{\text{aq}}$ , on the basis of triplicate control studies (Table EA1).

### 2.3. Aqueous constituent analyses

#### 2.3.1. Dissolved mercury

BrCl-digested samples were diluted in 0.1 N HCl for analysis using 0.13 M  $\text{SnCl}_2$  plus 0.12 M HCl reduction, purge and trap dual gold amalgamation, and cold vapor atomic fluorescence spectrometry (CVAFS). Fluorescence peak areas for five mercury standard solutions were measured in triplicate: one contiguous series at the beginning, a second set interspersed every 10–15 sample analyses, and a third contiguous series at the end of the analytical session. Hg standards were cross checked by solutions prepared from a different commercial standard stock and the NIST 1641d certified reference material. Dilution of samples prior to analysis introduced the most uncertainty in mercury concentrations, which was at most two percent on the basis of three replicate dilutions per dilution factor used per analysis session. All recoveries were corrected for trace amounts of mercury in BrCl reagent, which were determined in triplicate per analysis session in hydroxylamine hydrochloride-quenched 3 percent v/v BrCl solutions.

#### 2.3.2. Sulfide

During mercury phase-distribution experiments using  $\text{H}_2\text{S}_{(\text{g})}$ , S(-II) was measured *in situ* with a solid-state 100  $\mu\text{m}$ -diameter Hg/Au amalgam electrode, a double-junction Ag|AgCl|3 M KCl|0.1 M  $\text{NaNO}_3$  reference electrode, and a glassy carbon auxiliary electrode using stripping voltammetry (Davison and Gabbutt, 1979; Krznarić and Ciglencečki-Jušić, 2005). An Autolab PGSTAT12 potentiostat was used for all voltammetric measurements (Eco Chemie, Utrecht). Method details and quality assurance are provided in the Electronic annex.

### 2.4. Particle characterization

Dynamic light scattering (DLS) was measured at 20 °C with a Malvern Zetasizer nanoZS equipped with a 4 mW, 633 nm He–Ne laser and an avalanche photodiode detector oriented at 173° from the incoming path of the laser. Scattered photon intensity measurements were averaged over 10 s and convoluted into an intensity autocorrelation function ( $G_2(\tau)$ ), where  $\tau$  is the delay time of the digital correlator). Sixteen autocorrelation functions were collected and averaged per measurement.

Intensity autocorrelation functions were interpreted using a cumulants fit to a 3rd-order expansion of a quadratically weighted  $G_2(\tau)$  (Finsky, 1994). A second approach was to determine the distribution of particle sizes that optimally describes the DLS data using the CONTIN inversion-regularization algorithm (Provencher, 1979, 1982). CONTIN obtains an optimal fit to  $G_2(\tau)$  by compromising a least-squares minimization of fit residuals with a minimization of the curvature of the particle size distribution. The latter constraint is implemented using a regularizer ( $\alpha$ ) (Ruf, 1993).

### 2.5. Mercury speciation by X-ray absorption spectroscopy

Aqueous solutions of 10  $\mu\text{M}$  Hg, 10 (mg C)  $\text{L}^{-1}$  DOM, and 160  $\mu\text{M}$  S(-II) were allowed to react for 3–30 h. After these periods, samples were ultracentrifuged, then 80 percent of the liquid was removed and the remaining sample sonicated for 1 min to resuspend particles. These concentrates were transferred onto Kapton film sitting on a block of dry ice to slow further chemical reactions. The frozen concentrates were freeze-dried, smeared on the film with a spatula, and covered with Kapton tape for Hg-L<sub>III</sub> edge extended X-ray absorption fine structure (EXAFS) spectroscopic analysis. EXAFS was measured at room temperature on wiggler end-station 7-3 at the Stanford Synchrotron Radiation Lightsource (SSRL), a 3 GeV synchrotron operated at 100 mA. A harmonic rejection mirror was used to allow full tuning of the Si(2 2 0) monochromator. Fluorescence-yield data were collected with a 30-element solid-state germanium detector. The sample concentration procedure enabled sufficient signal-to-noise to obtain discernible EXAFS to  $k = 12 \text{ \AA}^{-1}$  by averaging 9–16 scans,  $k^2$ -weighting detector count times from 1 to 20 s across the EXAFS region ( $k$  is the photoelectron momentum). EXAFS spectra were extracted from the averaged data files by pre-edge subtraction followed by spline fitting using xafsX (Winterer, 1996).

The identity and molecular structure of mercury was determined from EXAFS by fitting Hg–S atomic pair correlations calculated using the *ab initio* code FEFF 7 (Zabinsky et al., 1995) to inverse-Fourier transforms of the first apparent Hg coordination shell. The amplitude reduction factor ( $S_0^2$ ) was fixed at 0.855 for all fits on the basis of the intersection of regressions of fitted Debye-Waller factors ( $\sigma^2$ ) versus  $S_0^2$  performed across multiple  $k$  weights of the EXAFS of metacinnabar. Four types of structural models were fit to the EXAFS spectra: (1) the standard harmonic model, (2) a split shell harmonic model, consisting of two overlapping pair correlations, (3) a cumulant expansion of the harmonic model, and (4) a model incorporating an asymmetric pair distribution function (Crozier et al., 1988). The harmonic and cumulant expansion models were fit using Artemis, a graphical interface for IFEFFIT (Ravel and Newville, 2005), whereas the analytical asymmetric model was fit using xafsX.

## 3. RESULTS

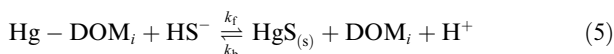
### 3.1. Phase distribution of mercury after sulfide addition to dissolved organic matter

#### 3.1.1. Apparent rate of sulfide-induced mercury precipitation and stability of $\text{HgS}_{(\text{s})}$

A general rate expression for the change in dissolved Hg ( $\text{Hg}_{\text{aq}}$ ) activity in the Hg–DOM–S(-II) system would be

$$\frac{d(\text{Hg}_{\text{aq}})}{dt} = -k_{\text{f}}(\text{HS}^-)^{\alpha} \prod_i^n (\text{Hg} - \text{DOM}_i)^{\gamma_i} + k_{\text{b}}(\text{HgS}_{(\text{s})})^{\beta} \prod_j^{n'} (\text{DOM}_j)^{\eta_j} \quad (4)$$

where  $t$  is the time since S(-II) amendment (seconds);  $k_f$  and  $k_b$  are the forward and backward rate coefficients of the reaction



the indices  $i$  and  $j$  represent one of  $n$  or  $n'$  types of Hg-DOM complexes or HgS<sub>(s)</sub>-dissolving DOM molecules; and  $\alpha$ ,  $\beta$ ,  $\gamma$ , and  $\eta$  are reaction coefficients. In these exploratory experiments, multiple constituents varied with time, and the stoichiometry of reactions between Hg<sup>2+</sup>, DOM components, Hg-DOM complexes, and S(-II) are unknown. Assuming negligible HgS<sub>(s)</sub> dissolution ( $k_b = 0$ ), the initial apparent rate at which Hg<sub>aq</sub> was lost from solu-

tion was computed on the basis of a simplified, closed-form rate expression:

$$\frac{d[\text{Hg}_{\text{aq}}]}{dt} = -k^*([\text{Hg}_{t=0}] - [\text{Hg}_{\text{non-labile}}]) \quad \text{which integrates to} \quad (6)$$

$$[\text{Hg}_{\text{aq}}] = ([\text{Hg}_{t=0}] - [\text{Hg}_{\text{non-labile}}]) \exp(-k^*t) \quad (7)$$

where  $k^*$  is a provisional first-order rate coefficient (s<sup>-1</sup>), Hg<sub>t=0</sub> is the initial concentration of Hg<sub>aq</sub> (assumed to be complexed by DOM), and Hg<sub>non-labile</sub> is the portion of Hg<sub>aq</sub> that does not readily react with S(-II).

Hg<sub>aq</sub> decreased approximately 80 percent over 1 h following the addition of 140 μM Na<sub>2</sub>S to 0.83 (mmol C) L<sup>-1</sup> SRFA solutions initially equilibrated with 2.28 × 10<sup>-3</sup> μM and 0.482 μM Hg (Fig. 1 and Table 1B and C). The initial pH of the Hg-SRFA solution was 7.0 and rose to pH 7.3 at the end of the experiment (Table 1). The rate Hg<sub>aq</sub> decreased upon addition of 140 μM Na<sub>2</sub>S to 0.482 μM Hg and SRFA is not statistically different at the 90 percent confidence level from the rate observed during the same S(-II) amendment to 1.0 μM Hg in the absence of DOM, on the basis of rate coefficients fit to the data using Eq. (7) (Table 1, experiments A and B). The initial Hg<sub>aq</sub> concentration did, however, significantly affect rates of Hg<sub>aq</sub> decrease: Hg<sub>aq</sub> decreased more slowly when 2.28 × 10<sup>-3</sup> μM Hg was initially present compared to 0.482 μM (Table 1A versus B and C). The Hg<sub>aq</sub> fraction that persisted (Hg<sub>non-labile</sub> in Eq. (7)) 1–7 h following sulfide amendment was 1.6–1.8 times higher when SRFA was present, after which the Hg<sub>aq</sub> fraction remained unchanged at 0.19 or 0.22—defined as Hg<sub>non-labile</sub> in Eqs. (6) and (7)—while it declined in the absence of DOM to 0.04 after 23 h (Fig. 1).

Results from two experiments in which less sulfide (as H<sub>2</sub>S<sub>(g)</sub>) was added to mixtures of 0.83 (mmol C) L<sup>-1</sup> SRFA and similar initial Hg concentrations (0.482–0.645 μM) are compared to the 140 μM Na<sub>2</sub>S amendment in Fig. 2. The pH of the reactors rose by as much as 0.3 as H<sub>2</sub>S and CO<sub>2</sub> partitioned into the aqueous phase (Table 1). S(-II) increased as H<sub>2</sub>S<sub>(g)</sub> partitioned into the aqueous phase,

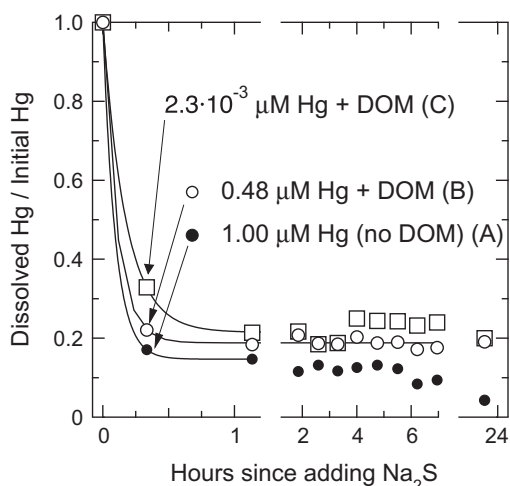


Fig. 1. Fraction of Hg<sub>aq</sub> following the addition of 140 μM Na<sub>2</sub>S in the presence of 0.83 mM C as Suwannee River fulvic acid. The letters in parentheses refer to experiment indices listed in Table 1. All data are normalized by the Hg<sub>aq</sub> measured in a sample taken just prior to adding S(-II), indicated by the arrows. Estimated variability in Hg<sub>aq</sub> recovery would plot smaller than the size of the symbols.

Table 1

Experimental conditions of the time-resolved Hg phase-distribution experiments, apparent rate of HgS<sub>(s)</sub> formation upon sulfide amendment to 0.83 mM C as Suwannee River fulvic acid (unless otherwise indicated), and the concentration of persistent dissolved Hg.  $k^*$  values are first-order rate coefficients during S(-II)-driven precipitation, after which the slopes of linear regressions and average Hg<sub>aq</sub> concentrations during a second reaction phase are listed (i.e., Hg<sub>non-labile</sub> in Eq. (7)).

Hg <sub>aq</sub> ( $t = 0$ ) (μM)	S(-II)	DOM	pH		Phase 1 $k^* \pm 90\%$ C.I. (s <sup>-1</sup> )	Phase 2 Slope $\pm 90\%$ C.I. (nM Hg s <sup>-1</sup> )	Hg <sub>non-labile</sub> (1σ)
			initial	final			
<i>Aqueous Na<sub>2</sub>S amendments</i>							
A 1.00	140 μM	no DOM	7.0	8.5	0.15 ± 0.03	–	0.12 (0.02)
B 0.482	140 μM	SRFA	7.0	7.4	0.16 ± 0.01	–	0.19 (0.01)
C 2.28 · 10 <sup>-3</sup>	140 μM	SRFA	7.0	7.4	0.12 ± 0.04	–	0.22 (0.02)
<i>H<sub>2</sub>S gas amendments</i>							
D 0.645	80 μM h <sup>-1</sup> → 120 μM	SRFA	7.3	7.5	0.08 ± 0.05	–0.02 ± 0.17	0.36 (0.03)
E 0.650	26 μM h <sup>-1</sup> → 25 μM	SRFA	7.0	7.3	0.05 ± 0.01	–	0.42 (0.03)
F 0.620	11 μM h <sup>-1</sup> → 6 μM	SRFA	6.9	7.2	0.07 ± 0.03	–0.16 ± 0.02	0.40 (0.03)
G 0.907	12 μM h <sup>-1</sup> → 9 μM	no DOM	7.3	7.5	0.13 ± 0.01	–	0.02 (0.003)
H 0.709	1.6 μM h <sup>-1</sup> → 1 μM	SRFA	7.3	5.9	0.09 ± 0.02	–0.47 ± 0.09	0.31 (0.06)

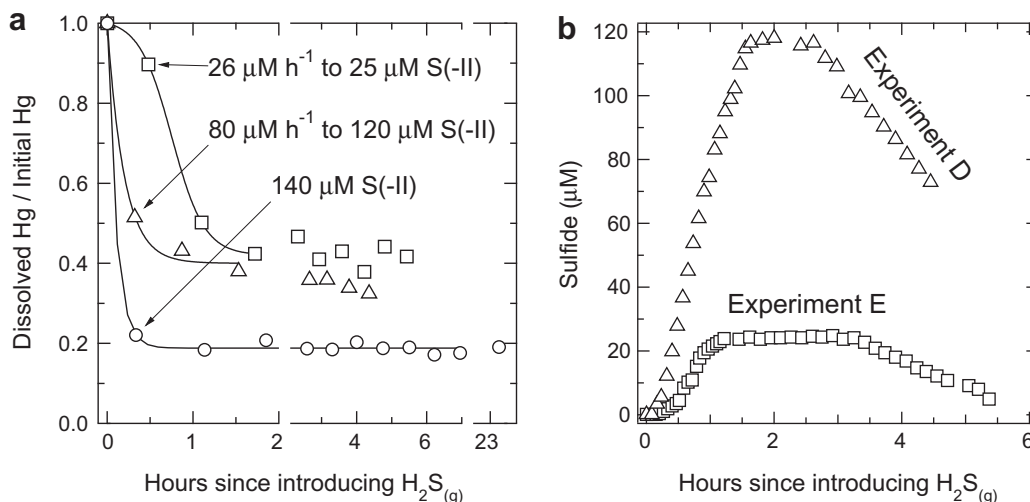


Fig. 2. (a) Fraction of Hg<sub>aq</sub> following the addition of H<sub>2</sub>S<sub>(g)</sub> in the presence of 0.83 mM C as Suwannee River fulvic acid. From bottom to top, the Hg<sub>aq</sub> concentrations measured in samples taken prior to adding S(-II) were 0.482, 0.645, and 0.650 μM, which all data are normalized by; (b) aqueous S(-II) concentration during experiments D and E, showing uptake of H<sub>2</sub>S<sub>(g)</sub> into the aqueous phase, plateau, and decrease primarily due to depletion of H<sub>2</sub>S<sub>(g)</sub> in the carrier gas as the S(-II) reservoir was depleted. 140 μM S(-II) was an instantaneous aqueous Na<sub>2</sub>S/H<sub>3</sub>BO<sub>3</sub> amendment (experiment B). Estimated variability in Hg<sub>aq</sub> recovery would plot smaller than the size of the symbols.

plateaued as partitioning and consumption balanced, and decreased primarily due to depletion of H<sub>2</sub>S<sub>(g)</sub> in the carrier gas as the S(-II) reservoir was depleted (Fig. 2b). The rate of S(-II) increase and its quasi-steady-state concentrations are listed in Table 1. In experiment D, Hg<sub>aq</sub> decreased significantly more slowly compared to when 140 μM Na<sub>2</sub>S was instantaneously added and, again, significantly more slowly in experiment E than D, on the basis of the 90-percent confidence intervals of fitted rate coefficients (Table 1). Hg<sub>aq</sub> concentrations between 2 and 6 h following the introduction of H<sub>2</sub>S<sub>(g)</sub> were, respectively, 1.9 and 2.2 times higher than that of the same period following 140 μM Na<sub>2</sub>S amendment (Table 1B, D and E), with approximately 40 percent Hg<sub>aq</sub> persisting (Fig. 2) as Hg<sub>non-labile</sub> (Eq. (7)).

In the previous two sets of experiments, S(-II) instantly or quickly exceeded Hg on the order of 10–100 times on a mole basis. A third set of experiments was conducted using H<sub>2</sub>S<sub>(g)</sub> at S(-II)-limited and near-limited conditions with similar SRFA and initial Hg concentrations. In experiment H, Hg<sub>aq</sub> decreased by 50 percent while S(-II) remained undetectable (<0.1 μM) for almost 30 min (Fig. 3). Hg<sub>aq</sub> temporarily stabilized at 0.27 μM while S(-II) reached 1 μM, after which S(-II) exceeded Hg<sub>aq</sub> and Hg<sub>aq</sub> more gradually decreased at  $0.47 \pm 0.09 \text{ nM s}^{-1}$ . The pH of the reactor decreased from 7.3 to 5.9 because the lower H<sub>2</sub>S concentration fed into the reactor was overcompensated by the concurrent CO<sub>2</sub> amendment of the reactor headspace.

In experiment F, where S(-II) exceeded Hg within 30 min and reached a S(-II)/Hg mole-ratio of 6, the initial rate at which Hg<sub>aq</sub> decreased is similar to experiment H (Fig. 3, open circles and diamonds). However, between 1 and 6 h after S(-II) introduction, Hg<sub>aq</sub> decreased at  $0.16 \pm 0.02 \text{ nM s}^{-1}$  in experiment F (6 μM peak S(-II)). That value is one third the rate observed when less S(-II) was in the reactor during experiment H (1 μM peak S(-II)). Under similar H<sub>2</sub>S<sub>(g)</sub> amendment conditions as exper-

iment F, the rate of Hg<sub>aq</sub> decrease was significantly faster in the absence of SRFA, with only two percent of Hg<sub>aq</sub> persisting (Hg<sub>non-labile</sub> in Eq. (7)) 1 h beyond the introduction of H<sub>2</sub>S<sub>(g)</sub> (experiment G in Table 1 and Fig. 3a).

### 3.1.2. Long term stability of mercury

Hg<sub>aq</sub> was periodically quantified for almost two weeks following the addition of 140 μM Na<sub>2</sub>S to 0.83 (mmol C) L<sup>-1</sup> solutions with Suwannee River fulvic and humic acid (SRFA and SRHA) and Pony Lake fulvic acid (PLFA). Five Hg concentrations over five orders of magnitude were studied for all three DOM isolates to determine how the Hg/DOM ratio—and therefore the strength of Hg–DOM association—would affect the solubility of Hg when Na<sub>2</sub>S was added.

In all fifteen cases (i.e., three DOM isolates by five Hg concentrations), Hg<sub>aq</sub> declined rapidly within 1 h following Na<sub>2</sub>S amendments, regardless of Hg concentration or type of DOM (Fig. 4). After this initial decline, however, Hg<sub>aq</sub> concentrations increased to varying degrees that are apparently sensitive to Hg concentration and type of DOM. For example, in the presence of 0.83 (mmol C) L<sup>-1</sup> SRFA and 518 nM Hg, Hg<sub>aq</sub> decreased by 85 percent 3 h after Na<sub>2</sub>S amendment but then almost tripled to 40 percent of the initial Hg<sub>aq</sub> 30 h later (Fig. 4a, second curve from the top). Starting with 1.11 nM Hg, an 80 percent Hg<sub>aq</sub> decline over 3 h was followed by complete dissolution of Hg (Fig. 4a, bottom curve), suggesting that the HgS<sub>(s)</sub> in this system dissolved to a greater extent than systems containing more Hg. Interestingly, in these and other cases, Hg<sub>aq</sub> declined again following dissolution. Staying with these same examples—518 and 1.11 nM Hg with SRFA and 140 μM S(-II)—Hg<sub>aq</sub> declined to 30 and 40 percent of their respective maxima at 30–40 h. Hg<sub>aq</sub> fluctuated during experiments with all DOM types and total Hg concentrations studied, cyclically in many cases. The pH of the reactors rose from pH 7 to

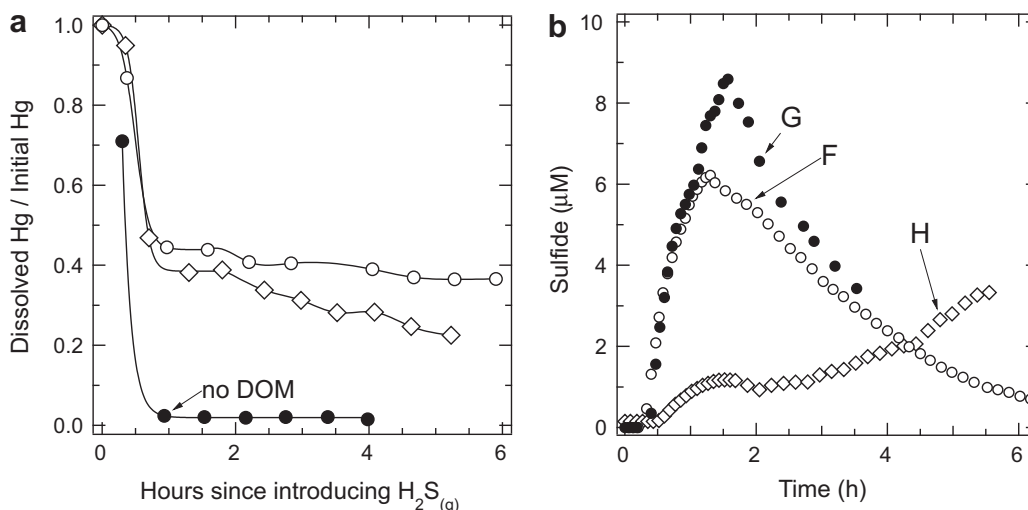


Fig. 3. (a) Fraction of  $Hg_{aq}$  following addition of S(-II) in the presence of 0.83 mM C as Suwannee River fulvic acid under sulfide-limited and near-limited conditions relative to the initial concentration of  $Hg_{aq}$  (from bottom to top, the initial  $Hg_{aq}$  measured in samples collected prior to adding S(-II) was 0.907  $\mu M$  (experiment G), 0.709  $\mu M$  (experiment H), and 0.620  $\mu M$  (experiment F), which all data were normalized by, (b) aqueous S(-II) concentration during these  $H_2S_{(g)}$ -amendment experiments;  $H_2S_{(g)}$  that partitioned into the aqueous phase was initially consumed (up to 30 min), presumably by reaction with  $Hg_{aq}$  and/or DOM, after which  $H_2S_{(g)}$  continued to partition into the aqueous phase, causing S(-II) to increase. In experiments F and G, S(-II) peaked and then decreased primarily due to depletion of  $H_2S_{(g)}$  in the carrier gas as the S(-II) reservoir was depleted. In experiment H, the S(-II) reservoir was not depleted; S(-II) was controlled instead by reactions with  $Hg_{aq}$  and/or DOM. Estimated variability in  $Hg_{aq}$  recovery would plot smaller than the size of the symbols.

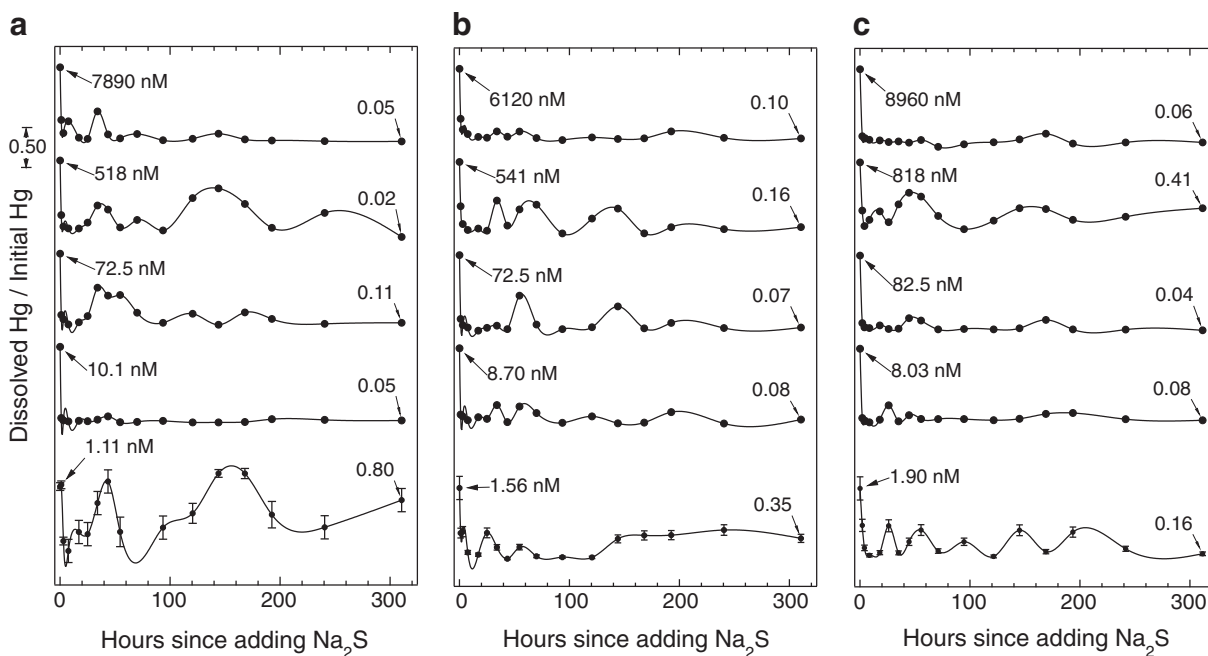


Fig. 4. Hg solubility over nearly two weeks following the addition of 140  $\mu M$   $Na_2S$  to 0.83 mM C solutions of (a) Suwannee River fulvic acid, (b) Suwannee River humic acid, and (c) Pony Lake fulvic acid, equilibrated with  $Hg(NO_3)_2$ . Curves are offset for clarity.  $Hg_{aq}$  concentrations measured prior to adding  $Na_2S$ , which all data are normalized by, are indicated by the arrows.  $Hg_{aq}$  fractions at the end of each experiment are also indicated. The scale bar to the left of panel (a) indicates a 50-percent change in the  $Hg(II)_{aq}$  fraction. Unless indicated otherwise, estimated variability in  $Hg_{aq}$  recovery would plot smaller than the size of the symbols.

7.8–7.9 in 1 day and pH 8.4–8.6 after 13 days, likely due to bisulfide buffering and DOM hydrolysis (Ritchie and Perdue, 2003).  $Hg_{aq}$  appears to have stabilized in about

12 of the 15 experiments, while three experiments suggest continual fluctuation after almost two weeks following  $Na_2S$  amendment. Apparently stable  $Hg_{aq}$  fractions ranged

from 0.02 to 0.35 (0.10 on average), depending on, but not systematically varying with, DOM type and total Hg concentration (Fig. 4). Since the solubility of  $\text{HgS}_{(s)}$  significantly increases above pH 8 (Clever et al., 1985), I cannot rule out enhanced Hg solubility due to elevated pH beyond 1 day following  $\text{Na}_2\text{S}/\text{H}_3\text{BO}_3$  amendment.

### 3.2. Mercury speciation and colloidal properties

Mercury L<sub>III</sub>-edge EXAFS analysis of freeze-dried ultracentrifugates of 10  $\mu\text{M}$  Hg, 0.83 (mmol C)  $\text{L}^{-1}$  DOM, and 160  $\mu\text{M}$  S(-II) mixtures indicate that Hg atoms are predominantly bonded to sulfur in condensed phases. Conceivable Hg–oxygen pair correlations overestimate amplitude in the 2–9  $\text{\AA}^{-1}$  region and so were not considered further. As shown in Fig. 5, the EXAFS amplitudes of Hg–S species formed in the presence of SRFA, SRHA, and, to a lesser extent, PLFA are less than that of crystalline metacinnabar ( $\beta\text{-HgS}$ ). In addition, Fourier transformed EXAFS reveal lower frequencies for Hg–S–DOM samples compared to  $\beta\text{-HgS}$  (Fig. 5b). The harmonic EXAFS structural model suggests that Hg atoms are surrounded on average by  $N = 2.5\text{--}3$  sulfur atoms at interatomic distances ranging from  $R = 2.34$  to 2.37  $\text{\AA}$  in three out of four Hg–S–DOM spectra, compared to 4 sulfurs at 2.53  $\text{\AA}$  for  $\beta\text{-HgS}$  (Table 2). Smaller coordination numbers and shorter interatomic distances are characteristic of the harmonic EXAFS model of disordered materials (Combes et al., 1989; Frenkel et al., 2001), as are higher Debye-Waller factors ( $\sigma^2$ ), which in the present study were 30% and 140% higher for the Hg–S pair correlation of Hg–S–DOM data compared to  $\beta\text{-HgS}$ . Three alternate models were employed to directly evaluate the disorder of the  $\text{HgS}_{(s)}$  species identified by EXAFS. For  $\beta\text{-HgS}$ , a split shell harmonic model consisting of two overlapping Hg–S pair correlations improved the reduced  $\chi^2$  ( $\chi_v^2$ ). The third cumulant ( $C_3$ ) of the expanded version of the harmonic model of  $\beta\text{-HgS}$  was zero within its standard deviation, reducing back to the standard harmonic model. The analytical asymmetric model of  $\beta\text{-HgS}$  produced the highest  $\chi_v^2$ , meaning the asymmetry parameter ( $h$ ) is unjustified. The split shell harmonic model of  $\beta\text{-HgS}$  closely matches its crystallographic structure and includes a  $\sigma^2$  value that is more typical of minerals, suggesting that the  $\beta\text{-HgS}$  sample is slightly disordered, which is conceivable for a heavy element in a specimen obtained from a mineral deposit. The least-squares optimized structural parameters of the cumulant expansion and analytical asymmetric models of  $\beta\text{-HgS}$  are in excellent agreement with crystallographic data (Table 2). Thus, while these latter two models are not statistically justified for  $\beta\text{-HgS}$ , they did not produce spurious structural parameters and so can be used to reliably assess the structure of  $\text{HgS}_{(s)}$  species formed in the presence of DOM.

Time of the reaction between 10  $\mu\text{M}$  Hg and 160  $\mu\text{M}$  S(-II) in the presence of SRFA improved EXAFS signal-to-noise (especially 9–12  $\text{\AA}^{-1}$ ; Fig. 5). The analytical asymmetric model of the Hg–S pair correlation was optimal for the sample quenched 3 h after S(-II) addition, considering the noise in the data and the plausibility of fitted  $\sigma^2$  and other structural variables (Table 2). After 30 h of reaction,

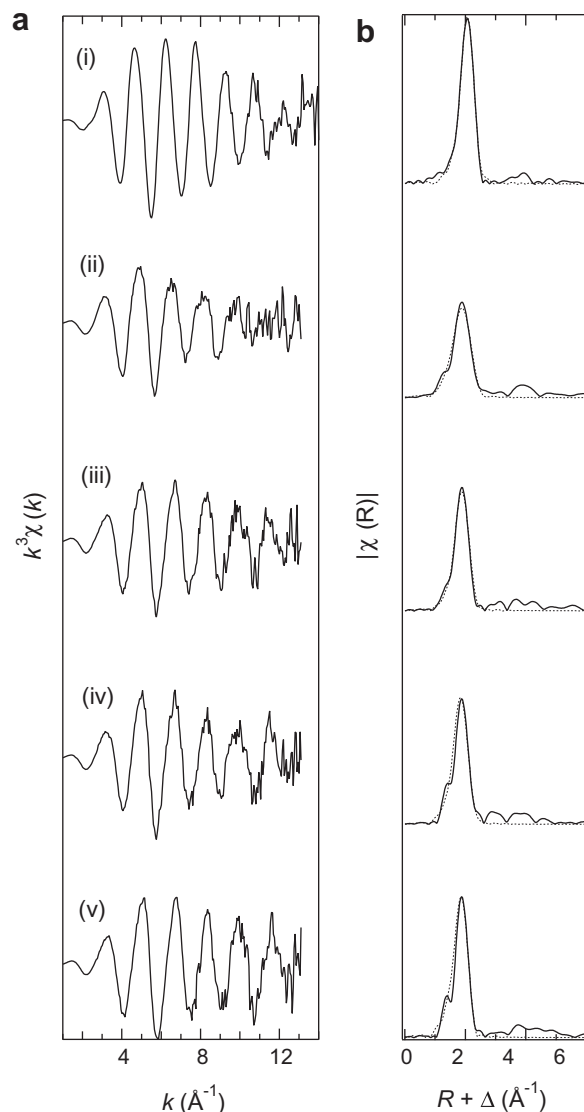


Fig. 5. (a) Hg-L<sub>III</sub> edge EXAFS and (b) radial structure functions of (i) crystalline metacinnabar and ultracentrifuged and lyophilized aqueous solutions that contained 10 (mg C)  $\text{L}^{-1}$ , 10  $\mu\text{M}$  Hg(II), and 160  $\mu\text{M}$  S(-II); (ii) SRFA quenched 3 h after adding S(-II), (iii) SRFA quenched 30 h after adding S(-II), (iv) SRHA quenched 30 h after adding S(-II), and (v) PLFA quenched 30 h after adding S(-II). (c) Inverse-Fourier transforms of the first Hg coordination shell; circles are the experimental data and lines are the optimal model summarized in Table 2.  $k$  is the momentum of the photoelectron wave,  $R$  is the average interatomic distance between Hg and surrounding backscattering atoms, and  $\Delta$  is the phase shift of the photoelectron wave as it interacts with the potentials of the Hg atoms and surrounding backscattering atoms, which typically ranges from 0.3 to 0.5  $\text{\AA}$ .

the split shell harmonic model fit is both reasonable and statistically optimal (Table 2). The analytical asymmetric model of the 3-h quenched sample suggests that Hg–S interatomic distances are initially broadly distributed and skewed upon S(-II) addition (Fig. 6) but then become shorter and less skewed after 30 h. The 3-h sample's Hg–S centroidal average interatomic distance ( $R$ ) is similar to that of

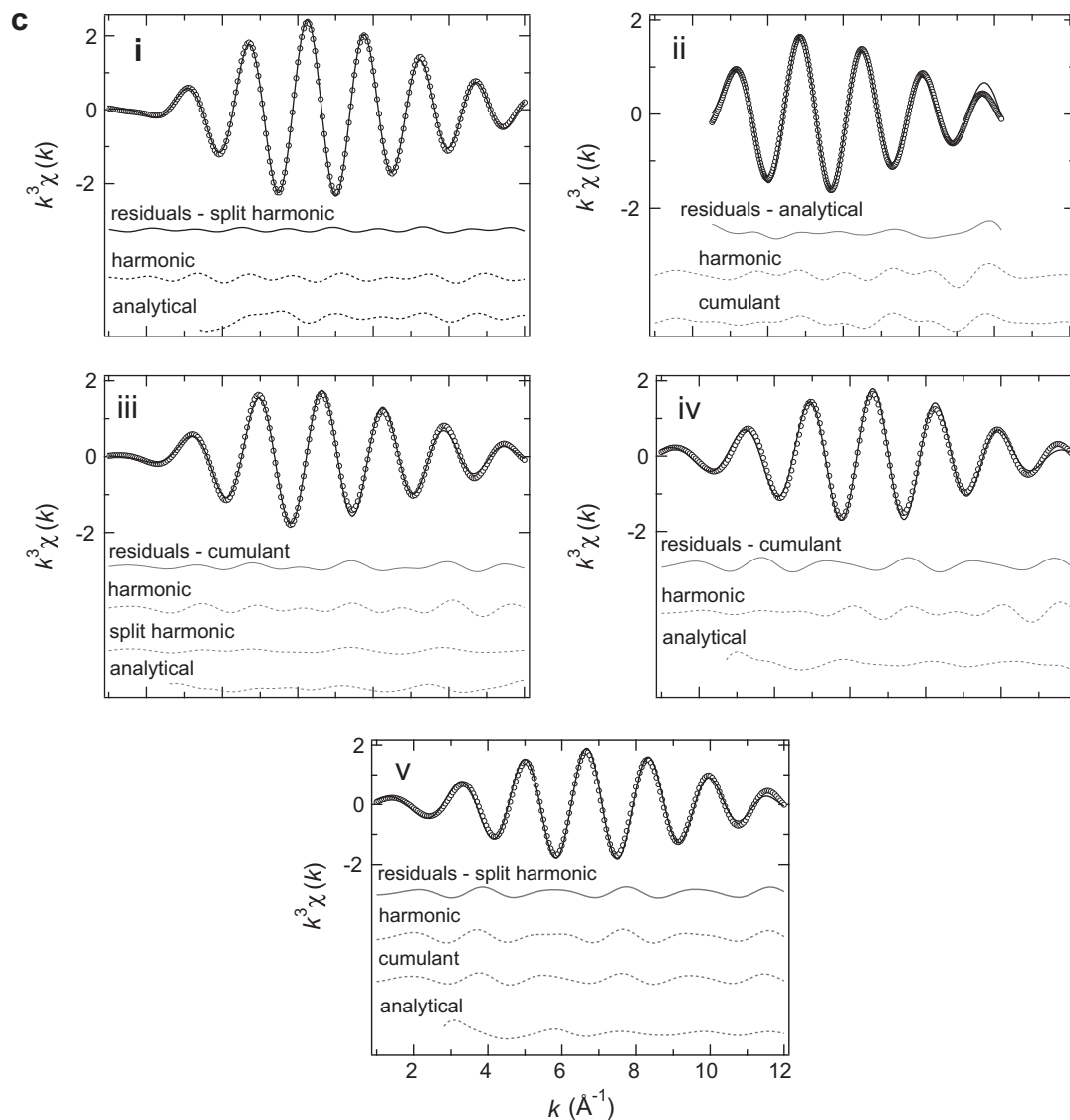


Fig. 5 (continued)

$\beta$ -HgS.  $R$  of the 30-h sample's Hg-S pair correlation is shorter ( $2.41 \pm 0.04 \text{ \AA}$ ) than  $\beta$ -HgS. While this interatomic distance resembles nearest neighbor sulfur atoms in cinnabar ( $\alpha$ -HgS), an  $\alpha$ -HgS Hg-S pair correlation fits the experimental EXAFS data poorly, further distinguishing the HgS<sub>(s)</sub> formed in the presence of SRFA from crystalline analogs. In addition, despite being more thermodynamically stable than  $\beta$ -HgS,  $\alpha$ -HgS does not form at room temperature (Hepler and Olofsson, 1975; Paquette and Helz, 1997). The 30-h sample's sulfur coordination number is significantly less than that of  $\beta$ -HgS. These results suggest that, upon S(-II) addition, Hg is primarily tetrahedrally coordinated by sulfur atoms with appreciable disorder on the molecular scale. As reactions between Hg, DOM, and S(-II) continued, the distribution of Hg-S interatomic distances narrowed while the weighted average Hg-S coordination number ( $N$ ) decreased.

This evolution of  $R$  and  $N$  is consistent with homogenization of the molecular structure of HgS<sub>4</sub> monomers

through limited polymerization; that is, polymerization was likely interrupted in the nanometer regime and did not attain the long-range structural order of crystalline  $\beta$ -HgS. Undercoordinated metal ions at particle surfaces (e.g., S-Hg-S) comprise a higher fraction of the total metal ions in nanoparticles (Frenkel et al., 2001). Assuming a spherical assemblage of HgS<sub>4</sub> monomers as in  $\beta$ -HgS, the 30-h reacted SRFA sample's coordination number ( $N = 2.9 \pm 0.5$ ) is consistent with a 1–2 nm HgS<sub>(s)</sub> polymer, which would have an average 2.5–3.2 sulfurs per Hg atom. Particle size determination on the basis of first shell EXAFS fitting is highly uncertain. Unfortunately, attempts to measure HgS<sub>(s)</sub> particle size in Hg-S-SRFA specimens with transmission electron microscopy were unsuccessful, probably due to volatilization of mercury, which I observed when examining synthetic  $\beta$ -HgS nanoparticles. Hg-S distances shorter than  $\beta$ -HgS could be due to surface and interior deformities caused by the presence of SRFA during HgS<sub>(s)</sub> precipitation, which has only been documented for

Table 2

First-shell fit results of Hg-L<sub>III</sub> edge extended X-ray absorption fine structure (EXAFS) of 10 (mg C)/L dissolved organic matter, 10 μM Hg(II) mixtures amended with 160 μM sulfide after ultracentrifugation and lyophilization.

Model	<i>N</i> <sup>a</sup>	<i>R</i> (Å) <sup>a</sup>	$\sigma^2$ (Å <sup>2</sup> )	<i>C</i> <sub>3</sub> (Å <sup>3</sup> × 10 <sup>-4</sup> )	<i>C</i> <sub>4</sub> (Å <sup>4</sup> × 10 <sup>-4</sup> )	<i>h</i> <sup>c</sup>	Δ <i>E</i> <sub>0</sub> (eV)	$\chi^2_v \times 10^{-2d}$
<i>Metacinnabarr</i> (β-HgS)								
Crystal data	4	2.531	–	–	–	–	–	–
Harmonic	4.0(5)	2.51(1)	0.010(1)	–	–	–	–1(1)	1.7
Split harmonic <sup>b</sup>	4(1)	2.54(6)	0.007(3)	–	–	–	1.9	1.4
Analytical	4.4(3)	2.54(1)	0.007(1)	–	–	0.048(9)	1.5(7)	3.3
<i>Suwannee River fulvic acid, quenched 3 h after adding S(-II)</i>								
Harmonic	4.2(7)	2.43(1)	0.017(2)	–	–	–	–3(1)	1.7
Cumulant	3.9(5)	2.48(1)	0.016(2)	9(3)	–	–	0.04	1.3
Analytical	4.5(6)	2.50(3)	0.009(1)	–	–	0.085(2)	1.7	2.2
<i>Suwannee River fulvic acid, quenched 30 h after adding S(-II)</i>								
Harmonic	2.5(3)	2.37(1)	0.010(1)	–	–	–	–5.3	1.2
Split harmonic	2.9(5)	2.41(4)	0.007(2)	–	–	–	–2.1	0.26
Cumulant	2.5(3)	2.41(1)	0.009(1)	5(2)	–	–	–2.1	0.40
Cumulant	3.3(3)	2.41(1)	0.015(1)	6.0(7)	1.4(3)	–	–2.1	0.52
Analytical	3.7(2)	2.50(1)	0.0030(4)	–	–	0.098(4)	2.5	1.5
<i>Suwannee River humic acid, quenched 30 h after adding S(-II)</i>								
Harmonic	3(2)	2.37(1)	0.012(6)	–	–	–	–5	9.0
Split harmonic	5(1)	2.40(2)	0.012(4)	–	–	–	–5	9.6
Cumulant	3(1)	2.40	0.011(3)	7(2)	–	–	–5	0.96
Analytical	5(1)	2.6(1)	0.004(1)	–	–	0.12(2)	5(1)	6.0
<i>Pony Lake fulvic acid, quenched 30 h after adding S(-II)</i>								
Harmonic	2.9(3)	2.34(2)	0.009(6)	–	–	–	–9(4)	7.0
Split harmonic	3.8(5)	2.38(1)	0.009(2)	–	–	–	–5	5.3
Cumulant	2.6(5)	2.38	0.008(2)	5.7(8)	–	–	–5	5.3
Analytical	4.2(4)	2.52(1)	0.0014(5)	–	–	0.109(6)	5	7.4

The standard deviations are listed in parentheses, representing the errors in the last digit.

<sup>a</sup> Coordination number (*N*) and weighted average interatomic distance (*R*), based on FEFF 7 Hg–S path generated from the β-HgS crystal structure.

<sup>b</sup> Two harmonic paths,  $N = N_1 + N_2$ ;  $R = \frac{R_1 N_1 + R_2 N_2}{N_1 + N_2}$ .

<sup>c</sup> Asymmetry parameter.

<sup>d</sup> Reduced  $\chi^2$  goodness-of-fit parameter:  $\chi^2_v = \frac{n_{\text{indp}}}{v-n} \sum_{i=1}^n (k^3 \hat{\chi}(k) - k^3 \chi_{\text{fit}}(k))^2$ , where  $n_{\text{indp}}$  is the number of independent points  $\frac{2\Delta k \Delta R}{\pi}$ ,  $v$  is the degrees of freedom of the fit  $v = n_{\text{indp}} - n_{\text{variables}}$ ,  $n$  is the total number of data points,  $\hat{\chi}(k)$  and  $\chi_{\text{fit}}(k)$  are the inverse Fourier transformed experimental data and fit, respectively, and  $k$  is the photoelectron momentum.

metal-sulfide nanoparticles produced with synthetic organic ligands (Gilbert and Banfield, 2005). To my knowledge, these data provide the first direct evidence for aggregated, DOM-coated HgS<sub>(s)</sub> nanoparticles since this model was proposed over 10 years ago (Ravichandran et al., 1999).

EXAFS analysis of the sample quenched 30 h after adding 160 μM S(-II) to 10 μM Hg and Suwannee River humic acid (SRHA) indicates the formation of a condensed HgS<sub>(s)</sub> phase having similar weighted average *N* and *R* as that formed in the presence of the fulvic acid isolate from the same natural water. However, the Hg–S–SRHA sample is best fit by the cumulant model, which implies greater structural disorder than the split shell model that optimally fitted the Hg–S–SRFA sample. An average coordination number of  $N = 3 \pm 1$  suggests that HgS<sub>(s)</sub> formed in the presence of SRHA may consist of small nanometer-scale polymers, but this finding is considerably uncertain given the 33% standard deviation of *N*.

Like the Hg–S–SRFA sample quenched 30 h after S(-II) addition, the similarly quenched Hg–S–Pony Lake fulvic acid (PLFA) sample's EXAFS is best fit by a split shell har-

monic model with  $N = 3.8$ , similar to β-HgS, and  $R = 2.38$  Å, which is significantly shorter than that of β-HgS and similar (within error) to *R* of the Hg–S–SRFA sample (Table 2). The single harmonic and cumulant fits also produced *R* values at least 0.16 Å shorter than their corresponding values of β-HgS fits, suggesting a distinct HgS<sub>(s)</sub> structure formed in the presence of PLFA.

Dynamic light scattering intensities for 0.83 (mmol C) L<sup>-1</sup> DOM, 10 mM NaHCO<sub>3</sub>, and 7–9 mM HClO<sub>4</sub> (pH 7) solutions were 25, 45, and 35 ± 5 kcps for SRFA, SRHA, and PLFA solutions, compared to 10 kcps for water alone. The addition of 10 μM Hg(NO<sub>3</sub>)<sub>2</sub> to any of these DOM solutions (aged for several weeks) did not significantly change scattered photon intensities. For a few hours following the addition of 140 μM Na<sub>2</sub>S to these Hg–DOM solutions, scattered photon intensities increased by a few to as much as 10 kcps (Table EA2). Unlike DOM or Hg–DOM solutions, the DLS intensity autocorrelation functions of S(-II)-amended samples had flat baselines, suggesting the formation of particles as confirmed by ultracentrifugation/chemical analysis and EXAFS.

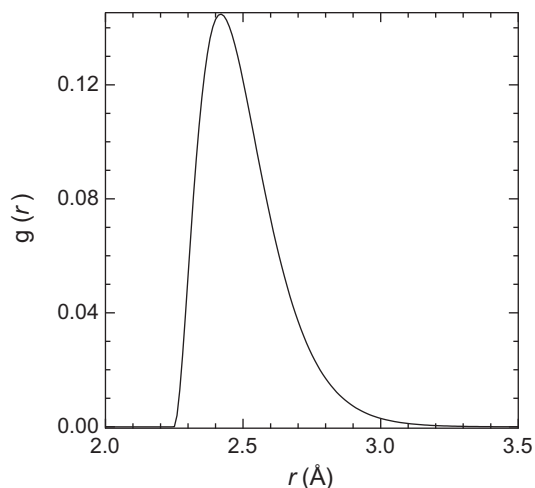


Fig. 6. Analytical pair distribution function included in the optimal fit of the Hg-S pair correlation of the sample quenched 3 h after adding 160  $\mu\text{M}$  S(-II) to 10  $\mu\text{M}$  Hg(II) and 0.83 mM C as Suwannee River fulvic acid. The interatomic distance ( $R$ ) is equivalent to the centroid of the distribution.  $h$  is the asymmetry parameter and  $N$  is the weighted average Hg-S coordination number.

Cumulants analysis of the autocorrelation functions excluded noisy data at short delay times, as shown by the left-most dotted lines in Fig. EA2. Chi-squared ( $\chi^2$ ) cumulants fit errors starting at those delay times and carried out until  $G_2(\tau)$  decayed to 0.1 of its initial value were, on average ( $\pm 1\sigma$  in the last digit), 0.009(2), 0.016(8), and 0.008(3) for SRFA, SRHA, and PLFA, respectively. An error  $\leq 0.005$  indicates a good fit, according to Malvern Instruments. Accordingly, I fit a truncated range of  $G_2(\tau)$  such that the fit error was approximately 0.005, yielding first cumulants in the colloidal size range with high polydispersity indices that preclude meaningful particle size determination. Particle size distributions (PSD) determined by the CONTIN algorithm for these DLS data are nano-to-colloidal in size (10–500 nm), do not corroborate first cumulants results, and suggest that particles were removed from the laser path by settling or adhesion to cuvette walls (Fig. EA2 and Table EA2).

DLS signal-to-noise improved substantially from Hg-DOM samples that were reacted with S(-II) for one day and inverted by hand immediately prior to DLS analysis (Fig. 7a). The first cumulants and dimensionless polydispersity indices (in parentheses) of the 10  $\mu\text{M}$  Hg(II) and 180  $\mu\text{M}$  S(-II)-bearing SRFA, SRHA, and PLFA solutions are 28 nm (0.27), 20 nm (0.001), and 22 nm (0.31), respectively. Cumulants fit  $\chi^2$  values were 0.002 or less. CONTIN particle size distributions, shown in Fig. 7b, include sizes indicated by first cumulants, but suggest a broader size distribution including particles as large as 200 nm.

#### 4. DISCUSSION

##### 4.1. Recovery of dissolved mercury

The initial rate at which  $\text{Hg}_{\text{aq}}$  is removed from solution primarily corresponds to the rate of  $\text{HgS}_{(\text{s})}$  formation. On

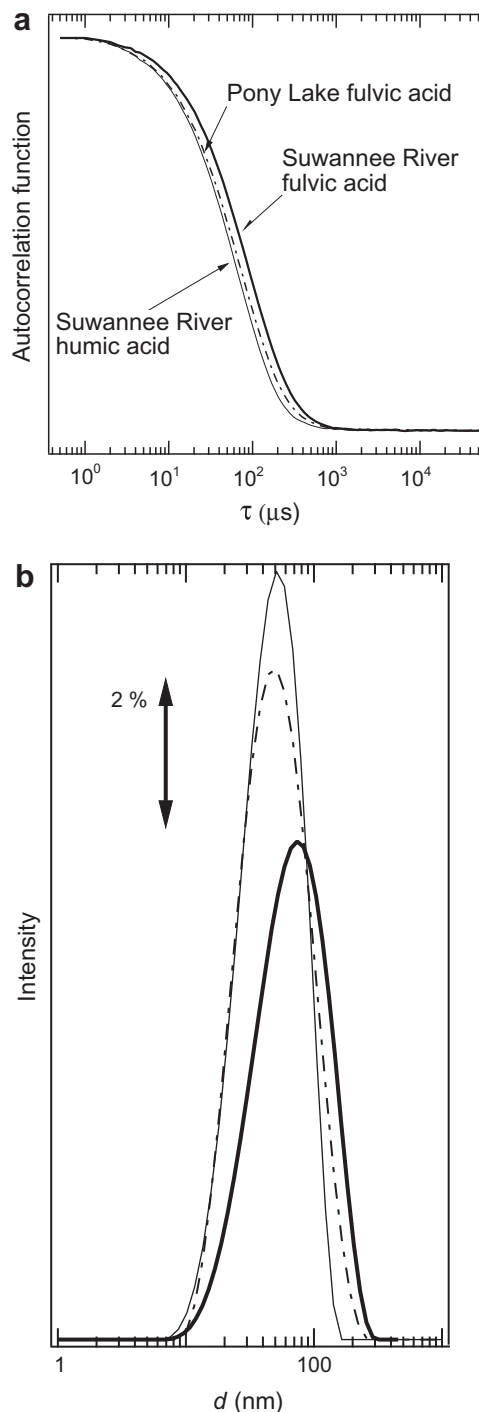


Fig. 7. (a) Dynamic light scattering intensity autocorrelation functions measured 24 h following the addition of 180  $\mu\text{M}$   $\text{Na}_2\text{S}$  to mixtures of 10  $\mu\text{M}$  Hg(II) and 0.83 mM C as Suwannee River fulvic acid, Suwannee River humic acid, and Pony Lake fulvic acid. (b) CONTIN particle size distributions.  $\tau$  is the delay time of the digital correlator;  $d$  is the spherical hydrodynamic diameter.

the basis of EXAFS spectroscopy, the formation of  $\text{HgS}_{(\text{s})}$  phases of varying structural disorder is unequivocal for systems containing 10  $\mu\text{M}$  Hg (Fig. 5 and Table 2).  $\text{HgS}_{(\text{s})}$  formation in systems containing less Hg is inferred from the

similar rates at which  $Hg_{aq}$  was lost from solution as the initial  $Hg_{aq}$  concentration decreased across five orders of magnitude (Table 1 and Figs. 1–4). In addition to the precipitation of  $Hg_{aq}$  as  $HgS_{(s)}$ , the decline of  $Hg_{aq}$  shown in Figs. 1–4 could include adhesion of  $Hg_{aq}$  to the walls of ultracentrifuge tubes, sorption of  $Hg_{aq}$  onto  $HgS_{(s)}$  surfaces, and settling by ultracentrifugation. The extent of adhesion in the absence of S(-II) is  $30 \pm 2\%$ , with an additional  $5 \pm 5\%$   $Hg_{aq}$  removed by ultracentrifugation from SRFA (details are provided in Annex). S(-II) likely outcompeted glass and polycarbonate for  $Hg_{aq}$ , so  $Hg_{aq}$  likely adhered less during the S(-II)-amended experiments. Even the greatest possible extent of  $Hg_{aq}$  adhesion, as measured in the absence of S(-II), does not account for most of the observed changes in  $Hg_{aq}$ . In addition,  $Hg_{aq}$  recoveries by ultracentrifugation and chemical analysis from Hg–DOM solutions varied by 2–5 percent ( $2\sigma$ ), on the basis of triplicate control experiments (Table EA1). Changes in excess of this variability can be assumed, then, to be primarily due to the precipitation or dissolution of  $HgS_{(s)}$ . The remainder of the discussion examines how DOM, Hg concentration, and S(-II) concentration affect changes in  $Hg_{aq}$  and therefore,  $HgS_{(s)}$  formation and stability over time-scales of hours to days, after which the importance of experimental parameters is discussed.

#### 4.2. Effect of Suwannee River fulvic acid and initial mercury concentration on $HgS_{(s)}$ formation

The initial rate of  $HgS_{(s)}$  formation is statistically indistinguishable in the presence or absence of SRFA upon addition of a 290-fold molar excess of S(-II) ( $140 \mu M$ ) to Hg at  $0.58 \mu mol Hg (mmol C)^{-1}$  (Fig. 1, experiment B). SRFA did, however, double the apparent solubility of Hg 1–7 h following  $Na_2S$  addition (Fig. 1, experiments B and C versus A). Twenty percent of Hg persisted in the dissolved phase for nearly a day in the presence of SRFA, while  $Hg_{aq}$  declined to 4 percent over the same period in the absence of SRFA. The 20 percent of persistent  $Hg_{aq}$  ( $0.1 \mu M$ ) is less than half the organic reduced sulfur in SRFA ( $0.46 \mu M$ ) (Waples et al., 2005). Therefore, this non-reactive fraction could consist of Hg–thiol complexes (e.g.,  $Hg(RS)_2$ ).

The initial rate of  $HgS_{(s)}$  formation is slower upon addition of the same amount of S(-II) ( $140 \mu M$ ) to SRFA containing three orders of magnitude less Hg (i.e.,  $2.7 \times 10^{-3} (\mu mol Hg) (mmol C)^{-1}$ ; Fig. 1, experiments C and B), indicating that DOM can slow the initial reaction between S(-II) and Hg at lower Hg/DOM ratios. DOM can significantly reduce the initial rate of  $HgS_{(s)}$  formation if Hg/SRFA ratios are on the order of  $10^{-3} (\mu mol Hg) (mmol C)^{-1}$ , but not when this ratio is on the order of 0.1. Regardless of the Hg/DOM ratio, SRFA prevented as much as  $0.1 (\mu mol Hg) (mmol C)^{-1}$  from precipitating over a 1-day period following addition of a 102-fold molar excess of S(-II) to Hg, indicating that SRFA can form  $Hg_{aq}$  complexes that are inert to S(-II) under these conditions (Fig. 1, experiments B and C versus A). These findings demonstrate that greater Hg–DOM complex stability at lower Hg/DOM ratios (Haitzer et al., 2002) limits Hg reactivity toward S(-II). This limita-

tion, while observable, is not so great as to reasonably expect complete inhibition of  $HgS_{(s)}$  formation by aquatic DOM in natural interstitial waters, which might contain  $10^{-6} \mu M Hg$ , compared to the  $10^{-3}$  to  $1 \mu M Hg$  used in the current experiments. That is,  $HgS_{(s)}$  is likely to form in the presence of aquatic DOM and S(-II) in natural systems, even in remote aquatic habitat contaminated solely by atmospheric Hg deposition.

#### 4.3. Effect of sulfide concentration on $HgS_{(s)}$ formation

Comparison of time-resolved  $Hg_{aq}$  concentrations under variable S(-II) amendments reveals an additional type of  $Hg_{aq}$  species with respect to reactivity toward S(-II). Across a wide range of S(-II)/Hg ratios—290-fold excess down to equimolar S(-II)/Hg—approximately 60 percent, or  $0.45$ – $0.51 \mu mol Hg$  per  $mmol C$ , reacts to form  $HgS_{(s)}$  (Figs. 2 and 3). Invariance in the extent to which  $HgS_{(s)}$  is formed upon addition of a wide range of S(-II) confirms that the Hg–SRFA complexes can react with S(-II), as would be expected thermodynamically across the range of observed Hg–DOM stability (Haitzer et al., 2002). Another set of Hg species, approximately 20 percent, or  $0.1 \mu mol Hg$  per  $mmol C$ , is evident from higher persistent  $Hg_{aq}$  concentrations during gradual versus instantaneous S(-II) addition (upper 2 curves in Figs. 2a and 3a (experiments D, E, F, and H) versus the bottom curve in Fig. 2a (experiment B)). SRFA hindered these Hg species from reacting with S(-II) to an extent dependent on S(-II) concentration. This dependency is consistent with a continuum of Hg–DOM complex stability as has been determined for Hg and other metals (Filella et al., 1990; Buffle and Filella, 1995; Haitzer et al., 2002). In summary,  $Hg_{aq}$  can be divided into three species with respect to its reactivity toward S(-II):  $0.5 \mu mol Hg$  per  $mmol C$  (60 percent) that are reactive,  $0.1 \mu mol Hg$  per  $mmol C$  (20 percent) that are kinetically hindered, and another  $0.1 \mu mol Hg$  per  $mmol C$  (20 percent) that are inert to reaction with S(-II).

#### 4.4. Stability of $HgS_{(s)}$ formed in the presence of dissolved organic matter

##### 4.4.1. Short term stability of $HgS_{(s)}$

One to two hours following sulfide addition, Hg solubility was determined not only by S(-II)-driven formation of  $HgS_{(s)}$  but increasingly by  $HgS_{(s)}$  dissolution, on the basis of differences in  $Hg_{aq}$  across a lower range of S(-II) amendments. These differences in  $Hg_{aq}$ , amounting to at least  $10^{-9} M$ , cannot be accounted for solely by S(-II)-promoted  $HgS_{(s)}$  dissolution, which thermodynamic modeling suggests would produce  $10^{-11} M Hg_{aq}$  in equilibrium with metacinnabar. Therefore,  $HgS_{(s)}$  was dissolved primarily by DOM or organic sulfur compounds. As shown in Fig. 2 (experiments D versus E),  $Hg_{aq}$  was less beyond 1.5 h when more S(-II) was present (approaching  $120 \mu M$  compared to  $25 \mu M$ ). Notwithstanding this finding,  $Hg_{aq}$  data at lower S(-II)/Hg ratios—1 to  $6 \mu mol S(-II)$  per  $\mu mol Hg$  (Fig. 3, experiments F and H)—indicate a contrary trend in which Hg is more soluble in the presence of *more* S(-II) during the second phase following the initial S(-II)-driven  $HgS_{(s)}$  formation. S(-II)/Hg

ratios less than 2 resulted in a more steady and rapid decline of  $Hg_{aq}$  from 1.5 to 5 h than when S(-II) reached 120  $\mu M$  over the same period (Table 1, experiments D versus H).  $Hg_{aq}$  sampled while S(-II) more rapidly reached a 6-fold S(-II)/Hg ratio is consistent with this counterintuitive trend (Fig. 3, experiments F and H). While the initial and final pH of experiments D and F are comparable (7.1 and  $7.4 \pm 0.2$ ), the low  $H_2S_{(g)}$  amendment in experiment H was overcompensated by  $CO_2$ , acidifying the reactor by 1.4 pH units (Table 1), possibly stabilizing  $HgS_{(s)}$ . Experiments D and F alone suggest that Hg is more soluble after  $HgS_{(s)}$  forms in 100-fold excess S(-II) compared to  $HgS_{(s)}$  formed in 6-fold excess S(-II).

One hypothesis for why  $HgS_{(s)}$  appears to be more soluble in the presence of more S(-II) is that  $HgS_{(s)}$  formed in the presence of higher S(-II) is subsequently dissolved more by SRFA or organic sulfur compounds formed by reactions between S(-II) and SRFA. EXAFS spectroscopy (Fig. 5) indicates that  $HgS_{(s)}$  nucleated in the presence of SRFA is more disordered than  $\beta$ - $HgS$  and suggests that it consists of 1–2 nm particles. DLS further suggests that these  $HgS_{(s)}$  particles are subunits within 20–200 nm aggregates. The ability of DOM moieties to stabilize or dissolve  $HgS_{(s)}$  in the molecular vicinity of nucleation sites may control the extent and rate of  $HgS_{(s)}$  dissolution after its initial rapid precipitation. Higher S(-II) concentrations will react with stronger Hg–DOM complexes (Fig. 2), detaching  $Hg^{2+}$  and freeing strongly binding ligands temporarily. Opportunistic adsorption of strong organic ligands such as hydrophobic moieties is expected to promote  $HgS_{(s)}$  disaggregation and dissolution (Ravichandran et al., 1998, 1999; Waples et al., 2005). Conversely,  $HgS_{(s)}$  formation driven by less S(-II) would limit reactions to more labile Hg–DOM complexes, limiting DOM adsorption to weaker ligands in the diffusion layer around  $HgS_{(s)}$  particles that are not associated with hydrophobic moieties. These weakly interacting ligands dissolve  $HgS_{(s)}$  less, resulting in greater aggregation and lower apparent Hg solubility.

#### 4.4.2. Long term stability of $HgS_{(s)}$

Periodic  $Hg_{aq}$  fluctuations observed on timescales of days (Fig. 4) reflect slow transformations of constituents that promote or hinder  $HgS_{(s)}$  dissolution. These transformations may have included addition of S(-II) into DOM to form organic polysulfides (Heitmann and Blodau, 2006), as suggested by suppressed S(-II) concentrations in the presence of SRFA (Fig. 3b, experiments F versus G). Organic molecules that hinder  $HgS_{(s)}$  dissolution (Waples et al., 2005) may have competed with  $HS^-$  for  $HgS_{(s)}$  surface sites, limiting the extent to which S(-II) dissolved  $HgS_{(s)}$  (Jay et al., 2000). The apparent effect of total Hg concentration and source of DOM on the magnitude of  $Hg_{aq}$  fluctuations is likely controlled by the size of  $HgS_{(s)}$  aggregates and abundance of dissolution-enhancing DOM components. While EXAFS and DLS suggest  $HgS_{(s)}$  nanoparticles form aggregates on the order of 100 nm, greater  $HgS_{(s)}$  dissolution in systems containing 0.001  $\mu M$  versus higher concentrations of Hg suggests that  $HgS_{(s)}$  nanoparticle aggregates were unstable, releasing  $HgS_{(s)}$  nanoparticles that are readily dissolved by DOM.

Dissolved-phase and interfacial reactions between Hg, DOM, and S(-II) introduce significant variability among findings of model-system research. For instance, DLS intensities in my experiments were less than those of Deonarine and Hsu-Kim (2009) even though concentrations of Hg and S(-II) were, respectively, three and 50 times higher in the current study. The lower DLS intensities in the present study might have been due to the formation of smaller or more polydisperse aggregates. Aside from different Hg and S(-II) concentrations, Hg was allowed to react with DOM for at least 11 h prior to adding S(-II) compared to 5 min in experiments by Deonarine and Hsu-Kim (2009). The apparent thermodynamic stability of Hg(II) has been shown to increase (Gasper et al., 2007) and reactivity decrease (Miller et al., 2009) over several hours, presumably as stronger, less abundant  $Hg^{2+}$ -binding ligands (e.g., thiols) replace weaker carboxyls. The importance of these strong Hg–DOM interactions to  $HgS_{(s)}$  instability is underscored by EXAFS evidence of structural and colloidal transformation in the  $HgS_{(s)}$ –SRFA systems quenched 3 and 30 h following S(-II) addition. Arguably, in near-surface sediments prone to redox fluctuation and found to favor methylmercury production (Hollweg et al., 2009), Hg(II) will bind with strong DOM ligands as sulfur is transformed.

## 5. CONCLUSIONS

Investigations of metal reactivity towards assessing metal bioavailability in soils and sediments are increasingly considering DOM. Compared to soil organic matter, there are few studies of the properties of aquatic DOM. The properties of soil organic matter are sometimes appropriated into conceptual models of metal–organic interactions in aquatic systems, ignoring important physicochemical differences between soils and aquatic organic matter resulting from, for example, preferential adsorption of aromatic and hydrophobic moieties by sediments (McKnight et al., 1992; Ochs et al., 1994) and the difference between the isolation of soil versus aquatic organic matter. To extract organic matter, soil is typically mixed with a strong hydroxide solution (Swift, 1996), whereas natural waters are acidified to pH 2, passed over chromatographic resin, and then eluted with 0.1 N NaOH (Aiken et al., 1992). A variety of techniques have been able to identify structural properties of soil organic matter because of its ability to form clusters (Sutton and Sposito, 2005), albeit when concentrations were, in some cases, unnaturally high (0.2–10 (g C)  $L^{-1}$ ). Studies of aquatic DOM, however, have provided no evidence for aggregation beyond 1–2 nm (Lead et al., 2000a,b; Reemtsma et al., 2008), even at concentrations as high as 10 (g C)  $L^{-1}$  (Aiken and Malcolm, 1987).  $HgS_{(s)}$  nanoparticles formed in my experiments may have adsorbed organic moieties to heteroaggregate SRFA, SRHA, and PLFA molecules, but this process is not likely to be measurable at  $\mu M$  Hg per mmol C ratios.

There is a disconnect between studies of overall Hg–DOM complexation and the properties of the tiny fractions of DOM that apparently affect Hg reactivity at  $HgS_{(s)}$  nucleation sites. We know that certain fractions of DOM

promote while others hinder cinnabar dissolution (Waples et al., 2005). We also know that S(-II) may chemically alter DOM (Heitmann and Blodau, 2006) and therefore should affect its reactivity with  $\text{HgS}_{(s)}$ . A Hg species distribution model needs to consider the stoichiometry of Hg–DOM reactions, which would require the ability to quantify specific DOM moieties. The stoichiometry of Hg reactions with soil organic matter ligands has been estimated on the basis of EXAFS spectroscopy (Skylberg, 2008), but no such spectroscopic evidence is likely forthcoming for dissolved Hg complexes with aquatic DOM. Reemtsma et al. (2008) derive compositions and structures using mass spectrometry following fractionation of soil and aquatic DOM by size-exclusion chromatography, but the proposed compounds do not contain nitrogen or sulfur, which should dominate  $\text{Hg}_{\text{aq}}$  species in organic-rich interstitial waters (Haitzer et al., 2002; Skylberg, 2008).

Next-generation species distribution models would also need to parameterize the effect of formation conditions on the kinetic or equilibrium coefficients of  $\text{HgS}_{(s)}$  dissolution reactions. The EXAFS results clearly suggest that DOM not only limits  $\text{HgS}_{(s)}$  particle growth to the nanometer regime, but also causes structural disorder. There is little basis to use metacinnabar as the dominant  $\text{HgS}_{(s)}$  species in a speciation model to predict Hg methylation under organic-rich, sulfate-reducing conditions.

Mercury uptake by bacterial cells as a necessary precursor to methylation are more likely to be controlled by kinetic (intermediate), not equilibrium, species. Although the rate of  $\text{HgS}_{(s)}$  formation depends on Hg/DOM and S(-II)/Hg ratios, it appears to be rapid enough to expect that S(-II) produced by sulfate-reducing bacteria will limit the amount of Hg accessible for methylation (Gilmour et al., 1998; Hammerschmidt et al., 2008; Mitchell and Gilmour, 2008). However, my results also show that up to 40 percent of Hg species ( $0.3 \mu\text{mol Hg per mmol C}$ ) can be hindered or prevented by DOM from reacting with S(-II) over several hours. The accessibility of these Hg–DOM species to methylating microorganisms remains unknown. Subsequent to initial S(-II)-driven  $\text{HgS}_{(s)}$  formation,  $\text{HgS}_{(s)}$  is susceptible to dissolution by DOM or organic sulfur species produced by addition of S(-II) to DOM, which could sustain levels of bioaccessible Hg that should be of ecological concern. Although not addressed in this study, cations such as  $\text{Ca}^{2+}$ ,  $\text{Mg}^{2+}$ , and  $\text{Al}^{3+}$  can inhibit DOM-promoted  $\text{HgS}_{(s)}$  dissolution (Ravichandran et al., 1998, 1999). This emerging kinetic conceptual model undermines the premise that the rate or extent of Hg methylation correlates to equilibrium Hg-species distributions.

#### ACKNOWLEDGMENTS

Experiments performed in this study were funded by a Mendhall Postdoctoral Fellowship with the Western Mineral and Environmental Science Center at the US Geological Survey. I thank Drs. George R. Aiken (USGS), James S. Kuwabara (USGS), Benjamin Gilbert (Lawrence Berkeley National Laboratory), and three anonymous reviewers for their forthright, careful reviews of this manuscript. Portions of this research were carried out at the Stanford Synchrotron Radiation Lightsource, a national user facility operated by Stanford University on behalf of the US Department

of Energy, Office of Basic Energy Sciences. Use of trade names in this paper is for identification purposes only and does not constitute endorsement by the US Geological Survey.

#### APPENDIX A. SUPPLEMENTARY DATA

Supplementary data associated with this article can be found, in the online version, at doi:10.1016/j.gca.2010.05.012.

#### REFERENCES

- Aiken G. R. and Malcolm R. L. (1987) Molecular weight of aquatic fulvic acids by vapor pressure osmometry. *Geochim. Cosmochim. Acta* **51**, 2177–2184.
- Aiken G. R., McKnight D. M., Thorn K. A. and Thurman E. M. (1992) Isolation of hydrophilic organic acids from water using nonionic macroporous resins. *Org. Geochem.* **18**, 567–573.
- Barnett M. O., Harris L. A., Turner R. R., Stevenson R. J., Henson T. J., Melton R. C. and Hoffman D. P. (1997) Formation of mercuric sulfide in soil. *Environ. Sci. Technol.* **31**, 3037–3043.
- Brown A., McKnight D. M., Chin Y., Roberts E. C. and Uhle M. (2004) Chemical characterization of dissolved organic material in Pony Lake, a saline coastal pond in Antarctica. *Mar. Chem.* **89**, 327–337.
- Buffle J. and Filella M. (1995) Physico-chemical heterogeneity of natural complexants: clarification. *Anal. Chim. Acta* **313**, 144–150.
- Buffle J. and Leppard G. G. (1995) Characterization of aquatic colloids and macromolecules. 2: Key role of physical structures on analytical results. *Environ. Sci. Technol.* **29**, 2176–2184.
- Chin Y., Aiken G. R. and O'Loughlin E. (1994) Molecular weight, polydispersity, and spectroscopic properties of aquatic humic substances. *Environ. Sci. Technol.* **28**, 1853–1858.
- Clever H. L., Johnson S. A. and Derrick M. E. (1985) The solubility of mercury and some sparingly soluble mercury salts in water and aqueous-electrolyte solutions. *J. Phys. Chem. Ref. Data* **14**, 631–681.
- Combes J., Manceau A., Calas G. and Bottero J. (1989) Formation of ferric oxides from aqueous solutions: a polyhedral approach by X-ray absorption spectroscopy. I: Hydrolysis and formation of ferric gels. *Geochim. Cosmochim. Acta* **53**, 583–594.
- Crozier E., Rehr J. J. and Ingalls R. (1988) Amorphous and liquid systems. In *X-ray Absorption. Principles, Applications, Techniques of EXAFS, SEXAFS and XANES* (eds. D. Koningsberger and R. Prins). John Wiley & Sons, New York.
- Daskalakis K. D. and Helz G. R. (1993) The solubility of sphalerite (ZnS) in sulfidic solutions at 25 °C and 1 atm pressure. *Geochim. Cosmochim. Acta* **57**, 4923–4931.
- Davison W. and Gabbutt C. D. (1979) Polarographic methods for measuring uncomplexed sulfide ions in natural waters. *J. Electroanal. Chem.* **99**, 311–320.
- Deonaraine A. and Hsu-Kim H. (2009) Precipitation of mercuric sulfide nanoparticles in NOM-containing water: implications for the natural environment. *Environ. Sci. Technol.* **43**, 2368–2373.
- Eagles-Smith C. A. and Ackerman J. T. (2009) Rapid changes in small fish mercury concentrations in estuarine wetlands: implications for wildlife risk and monitoring programs. *Environ. Sci. Technol.* **43**, 8658–8664.
- Filella M., Buffle J. and van Leeuwen H. P. (1990) Effect of physico-chemical heterogeneity of natural complexants Part I. Voltammetry of labile metal–fulvic complexes. *Anal. Chim. Acta* **232**, 209–223.

- Finsy R. (1994) Particle sizing by quasi-elastic light scattering. *Adv. Colloid Interface Sci.* **52**, 79–143.
- Fitzgerald W. F., Lamborg C. H. and Hammerschmidt C. R. (2007) Marine biogeochemical cycling of mercury. *Chem. Rev.* **107**, 641–662.
- Fleming E. J., Mack E. E., Green P. G. and Nelson D. C. (2006) Mercury methylation from unexpected sources: molybdate-inhibited freshwater sediments and an iron-reducing bacterium. *Appl. Environ. Microbiol.* **72**, 457–464.
- Frenkel A. I., Hills C. W. and Nuzzo R. G. (2001) A view from the inside: complexity in the atomic scale ordering of supported metal nanoparticles. *J. Phys. Chem. B* **105**, 12689–12703.
- Gaspar J. D., Aiken G. R. and Ryan J. N. (2007) A critical review of three methods used for the measurement of mercury ( $\text{Hg}^{2+}$ )-dissolved organic matter stability constants. *Appl. Geochem.* **22**, 1583–1597.
- Gilbert B. and Banfield J. F. (2005) Molecular-scale processes involving nanoparticulate minerals in biogeochemical systems. In *Molecular Geomicrobiology* (eds J. Banfield, J. Cervini-Silva and K. Nealson). Mineralogical Society of America and Geochemical Society, Virginia, pp. 109–155.
- Gilmour C., Riedel G., Ederington M., Bell J., Benoit J., Gill G. and Stordal M. (1998) Methylmercury concentrations and production rates across a trophic gradient in the northern Everglades. *Biogeochemistry* **40**, 327–345.
- Haitzer M., Aiken G. R. and Ryan J. N. (2002) Binding of mercury(II) to dissolved organic matter: the role of the mercury-to-DOM concentration ratio. *Environ. Sci. Technol.* **36**, 3564–3570.
- Haitzer M., Aiken G. R. and Ryan J. N. (2003) Binding of mercury(II) to aquatic humic substances: influence of pH and source of humic substances. *Environ. Sci. Technol.* **37**, 2436–2441.
- Hall B. D., Aiken G. R., Krabbenhoft D. P., Marvin-DiPasquale M. and Swarzenski C. M. (2008) Wetlands as principal zones of methylmercury production in southern Louisiana and the Gulf of Mexico region. *Environ. Pollut.* **154**, 124–134.
- Hammerschmidt C. R., Fitzgerald W. F., Balcom P. H. and Visscher P. T. (2008) Organic matter and sulfide inhibit methylmercury production in sediments of New York/New Jersey Harbor. *Mar. Chem.* **109**, 165–182.
- Han F. X. X., Shiyab S., Chen J., Su Y., Monts D. L., Waggoner C. A. and Matta F. B. (2008a) Extractability and bioavailability of mercury from a mercury sulfide contaminated soil in Oak Ridge, Tennessee, USA. *Water Air Soil Pollut.* **194**, 67–75.
- Han S., Obratsova A., Pretto P., Deheyn D. D., Gieskes J. and Tebo B. M. (2008b) Sulfide and iron control on mercury speciation in anoxic estuarine sediment slurries. *Mar. Chem.* **111**, 214–220.
- Hedges J. I. and Oades J. M. (1997) Comparative organic geochemistries of soils and marine sediments. *Org. Geochem.* **27**, 319–361.
- Heitmann T. and Blodau C. (2006) Oxidation and incorporation of hydrogen sulfide by organic matter. *Chem. Geol.* **235**, 12–20.
- Hepler L. G. and Olofsson G. (1975) Mercury—thermodynamic properties, chemical-equilibria, and standard potentials. *Chem. Rev.* **75**, 585–602.
- Hollweg T. A., Gilmour C. C. and Mason R. P. (2009) Methylmercury production in sediments of Chesapeake Bay and the mid-Atlantic continental margin. *Mar. Chem.* **114**, 86–101.
- Jay J. A., Morel F. M. M. and Hemond H. F. (2000) Mercury speciation in the presence of polysulfides. *Environ. Sci. Technol.* **34**, 2196–2200.
- Kalbitz K., Solinger S., Park J. H., Michalzik B. and Matzner E. (2000) Controls on the dynamics of dissolved organic matter in soils: a review. *Soil Sci.* **165**, 277–304.
- Kim C. S., Brown, Jr., G. E. and Rytuba J. J. (2000) Characterization and speciation of mercury-bearing mine wastes using X-ray absorption spectroscopy XAS. *Sci. Total Environ.* **261**, 157–168.
- Kim C. S., Rytuba J. J. and Brown, Jr., G. E. (2004) Geological and anthropogenic factors influencing mercury speciation in mine wastes: an EXAFS spectroscopy study. *Appl. Geochem.* **19**, 379–393.
- King J. K., Kostka J. E., Frischer M. E., Saunders F. M. and Jahnke R. A. (2001) A quantitative relationship that demonstrates mercury methylation rates in marine sediments are based on the community composition and activity of sulfate-reducing bacteria. *Environ. Sci. Technol.* **35**, 2491–2496.
- Krznarić D. and Ciglenceki-Jusić I. (2005) Electrochemical processes of sulfide in NaCl electrolyte solutions on mercury electrode. *Electroanalysis* **17**, 1317–1324.
- Lead J. R., Wilkinson K. J., Balnois E., Cutak B. J., Larive C. K., Assemi S. and Beckett R. (2000a) Diffusion coefficients and polydispersities of the Suwannee River fulvic acid: comparison of fluorescence correlation spectroscopy, pulsed-field gradient nuclear magnetic resonance, and flow field-flow fractionation. *Environ. Sci. Technol.* **34**, 3508–3513.
- Lead J. R., Wilkinson K. J., Starchev K., Canonica S. and Buffle J. (2000b) Determination of diffusion coefficients of humic substances by fluorescence correlation spectroscopy: role of solution conditions. *Environ. Sci. Technol.* **34**, 1365–1369.
- Liu G. L., Cabrera J., Allen M. and Cai Y. (2006) Mercury characterization in a soil sample collected nearby the DOE Oak Ridge Reservation utilizing sequential extraction and thermal desorption method. *Sci. Total Environ.* **369**, 384–392.
- Malcolm R. L., McKnight D. M. and Averett R. C. (1994) History and description of the Okefenokee Swamp—Origin of the Suwannee River. In *Humic Substances in the Suwannee River, Georgia: Interactions, Properties, and Proposed Structures* (eds R. C. Averett, J. A. Leenheer, D. M. McKnight and K. A. Thorn). United States Geological Survey, Denver, Colorado, pp. 1–12.
- Marvin-DiPasquale M., Lutz M. A., Brigham M. E., Krabbenhoft D. P., Aiken G. R., Orem W. H. and Hall B. D. (2009) Mercury cycling in stream ecosystems. 2. Benthic methylmercury production and bed sediment pore water partitioning. *Environ. Sci. Technol.* **43**, 2726–2732.
- McKnight D. M., Bencala K. E., Zellweger G. W., Aiken G. R., Feder G. L. and Thorn K. A. (1992) Sorption of dissolved organic-carbon by hydrous aluminum and iron-oxides occurring at the confluence of Deer Creek with the Snake River, Summit County, Colorado. *Environ. Sci. Technol.* **26**, 1388–1396.
- Mergler D., Anderson H. A., Chan L. H. M., Mahaffey K. R., Murray M., Sakamoto M. and Stern A. H. (2007) Methylmercury exposure and health effects in humans: a worldwide concern. *Ambio* **36**, 3–11.
- Merritt K. A. and Amirbahman A. (2009) Mercury methylation dynamics in estuarine and coastal marine environments—a critical review. *Earth Sci. Rev.* **96**, 54–66.
- Miller C. L., Southworth G., Brooks S., Liang L. and Gu B. (2009) Kinetic controls on the complexation between mercury and dissolved organic matter in a contaminated environment. *Environ. Sci. Technol.* **43**, 8548–8553.
- Mitchell C. P. J. and Gilmour C. C. (2008) Methylmercury production in a Chesapeake Bay salt marsh. *J. Geophys. Res. Biogeo.* **113**.
- Ochs M., Cosovic B. and Stumm W. (1994) Coordinative and hydrophobic interaction of humic substances with hydrophilic  $\text{Al}_2\text{O}_3$  and hydrophobic mercury surfaces. *Geochim. Cosmochim. Acta* **58**, 639–650.

- Oiffer L. and Siciliano S. D. (2009) Methyl mercury production and loss in Arctic soil. *Sci. Total Environ.* **407**, 1691–1700.
- Paquette K. E. and Helz G. R. (1997) Inorganic speciation of mercury in sulfidic waters: The importance of zero-valent sulfur. *Environ. Sci. Technol.* **31**, 2148–2153.
- Provencher S. W. (1979) Inverse problems in polymer characterization: direct analysis of polydispersity with photon correlation spectroscopy. *Makromol. Chem.* **180**, 201–209.
- Provencher S. W. (1982) CONTIN: a general purpose constrained regularization program for inverting noisy linear algebraic and integral equations. *Comput. Phys. Commun.* **27**, 229–242.
- Ravel B. and Newville M. (2005) Athena, Artemis, Hephaestus: data analysis for X-ray absorption spectroscopy using IFEFFIT. *J. Synchrotron Rad.* **12**, 537–541.
- Ravichandran M. (2004) Interactions between mercury and dissolved organic matter—a review. *Chemosphere* **55**, 319–331.
- Ravichandran M., Aiken G. R., Reddy M. M. and Ryan J. N. (1998) Enhanced dissolution of cinnabar (mercuric sulfide) by dissolved organic matter isolated from the Florida Everglades. *Environ. Sci. Technol.* **32**, 3305–3311.
- Ravichandran M., Aiken G. R., Ryan J. N. and Reddy M. M. (1999) Inhibition of precipitation and aggregation of metacinnabar (mercuric sulfide) by dissolved organic matter isolated from the Florida Everglades. *Environ. Sci. Technol.* **33**, 1418–1423.
- Reemtsma T., These A., Springer A. and Linscheid M. (2008) Differences in the molecular composition of fulvic acid size fractions detected by size-exclusion chromatography-on line Fourier transform ion cyclotron resonance (FTICR-) mass spectrometry. *Water Res.* **42**, 63–72.
- Ritchie J. D. and Perdue E. M. (2003) Proton-binding study of standard and reference fulvic acids, humic acids, and natural organic matter. *Geochim. Cosmochim. Acta* **67**, 85–96.
- Ruf H. (1993) Data accuracy and resolution in particle sizing by dynamic light scattering. *Adv. Colloid Interface Sci.* **46**, 333–342.
- Schaefer J. K. and Morel F. M. M. (2009) High methylation rates of mercury bound to cysteine by *Geobacter sulfurreducens*. *Nat. Geosci.* **2**, 123–126.
- Scheuhammer A. M., Meyer M. W., Sandheinrich M. B. and Murray M. W. (2007) Effects of environmental methylmercury on the health of wild birds, mammals, and fish. *Ambio* **36**, 12–18.
- Skyllberg U. (2008) Competition among thiols and inorganic sulfides and polysulfides for Hg and MeHg in wetland soils and sediments under suboxic conditions: illumination of controversies and implications for MeHg net production. *J. Geophys. Res. Biogeo.* **113**, G00C03.
- Slowey A. J., Johnson S. B., Rytuba J. J. and Brown, Jr., G. E. (2005a) Role of organic acids in promoting colloid transport of mercury from mine tailings. *Environ. Sci. Technol.* **39**, 7869–7874.
- Slowey A. J., Rytuba J. J. and Brown, Jr., G. E. (2005b) Speciation of mercury and mode of transport from placer gold mine tailings. *Environ. Sci. Technol.* **39**, 1547–1554.
- Stewart A. R., Saiki M. K., Kuwabara J. S., Alpers C. N., Marvin-DiPasquale M. and Krabbenhoft D. P. (2008) Influence of plankton mercury dynamics and trophic pathways on mercury concentrations of top predator fish of a mining-impacted reservoir. *Can. J. Fish Aquat. Sci.* **65**, 2351–2366.
- Sutton R. and Sposito G. (2005) Molecular structure in soil humic substances: the new view. *Environ. Sci. Technol.* **39**, 9009–9015.
- Swift R. S. (1996) Organic matter characterization. In *Methods of Soil Analysis. Part 3: Chemical Methods* (eds. D. L. Sparks and J. M. Bartels). Soil Science Society of America, Madison, Wisconsin, pp. 1011–1069.
- Thurman E. M. (1985) Amount of organic carbon in natural waters. In *Organic Geochemistry of Natural Waters* (ed. E. M. Thurman). Kluwer Academic Publishers, Dordrecht, The Netherlands, pp. 273–361.
- Waples J., Nagy K. L., Aiken G. R. and Ryan J. N. (2005) Dissolution of cinnabar (HgS) in the presence of natural organic matter. *Geochim. Cosmochim. Acta* **69**, 1575–1588.
- Windham-Myers L., Marvin-DiPasquale M., Krabbenhoft D. P., Agee J. L., Cox M. H., Heredia-Middleton P., Coates C. and Kakouros E. (2009) Experimental removal of wetland emergent vegetation leads to decreased methylmercury production in surface sediment. *J. Geophys. Res. Biogeo.* **114**, G00C05.
- Winterer M. (1996) XAFS—a data analysis program for materials science. *J. Phys. IV* **7**, 243–244.
- Zabinsky S. I., Rehr J. J., Ankudinov A., Albers R. C. and Eller M. J. (1995) Multiple scattering calculations of X-ray absorption spectra. *Phys. Rev. B* **52**, 2995.

Associate editor: George R. Helz